TURUN YLIOPISTON JULKAISUJA
ANNALES UNIVERSITATIS TURKUENSIS

SARJA - SER. A I OSA - TOM. 471

ASTRONOMICA - CHEMICA - PHYSICA - MATHEMATICA

TWO-DIMENSIONAL ATOM LOCALIZATION AND RAMAN COOLING OF TRIPOD-TYPE ATOMS

by

Vladimir Ivanov

TURUN YLIOPISTO
UNIVERSITY OF TURKU
Turku 2013

From

Department of Physics and Astronomy
University of Turku
Finland

Supervised by

Kalle-Antti Suominen
Professor
Department of Physics and Astronomy
University of Turku
Finland

Reviewed by

Matti Kaivola
Professor
Department of Applied Physics
Aalto University School of Science
Finland

Vincent Boyer
Lecturer
School of Physics and Astronomy
University of Birmingham
United Kingdom

Opponent

Nikolay Vitanov
Professor
Department of Physics
Sofia University
Bulgaria

ISBN 978-951-29-5522-0 (PRINT)
ISBN 978-951-29-5523-7 (PDF)
ISSN 0082-7002
Painosalama Oy - Turku, Finland 2013

Acknowledgements

As each story has its beginning, my scientific research in the University of Turku started from the first visit to this amazing city and a meeting with Prof. Kalle-Antti Suominen. Initiated in 2009, this fruitful collaboration has numbered about five years and is summarized in the thesis.

I wish to thank especially my supervisor Prof. Kalle-Antti Suominen for all that he did for me. Your unconditional support within the scientific area and outside it has provided comfortable working facilities during all this time. My acknowledgements also go to Prof. Yuri Rozhdestvesky from Saint-Petersburg (Russia), who has rendered great influence on my scientific growth. I could not imagine this research finished without our thoughtful discussions.

Particular gratitude to Dr. Sergey Vasiliev for his aid in different worldly situations. My warmest thanks goes to friends and colleagues from the group in Turku: Jaakko Lehtinen, Lauri Toikka and Jaakko Lehto. With them, I enjoyed much more the time spending in the office.

In the end, I gratefully acknowledge financial support from the Finnish Academy of Science and Letters, CIMO, and the Academy of Finland.

Contents

Abstract

Both atom localization and Raman cooling, considered in the thesis, reflect recent progress in the area of all-optical methods. We focus on two-dimensional (2D) case, using a four-level tripod-type atomic scheme for atom localization within the optical half-wavelength as well as for efficient subrecoil Raman cooling.

In the first part, we discuss the principles of 1D atom localization, accompanying by an example of the measurement of a spontaneously-emitted photon. Modifying this example, one archives sub-wavelength localization of a three-level Λ-type atom, measuring the population in its upper state. We go further and obtain 2D sub-wavelength localization for a four-level tripod-type atom. The upper-state population is classified according to the spatial distribution, which in turn forms such structures as spikes, craters and waves.

The second part of the thesis is devoted to Raman cooling. The cooling process is controlled by a sequence of velocity-selective transfers from one to another ground state. So far, 1D deep subrecoil cooling has been carried out with the sequence of square or Blackman pulses, applied to Λ-type atoms. In turn, we discuss the transfer of atoms by stimulated Raman adiabatic passage (STIRAP), which provides robustness against the pulse duration if the cooling time is not in any critical role. A tripod-type atomic scheme is used for the purpose of 2D Raman cooling, allowing one to increase the efficiency and simplify the realization of the cooling.

List of publications

This thesis consists of an introductory part, followed by five research publications.

I *Two-dimensional atom localization in a four-level tripod system in laser fields*
V. Ivanov and Yu. Rozhdestvensky
Physical Review A **81** (2010) 033809 (7 pages).

II *Theory of robust subrecoil cooling by stimulated Raman adiabatic passage*
V. S. Ivanov, Yu. V. Rozhdestvensky, and K.-A. Suominen
Physical Review A **85** (2012) 033422 (8 pages).

III *Momentum distribution of atoms in one-dimensional Raman cooling with arbitrary coherent population transfer*
V. S. Ivanov and K.-A. Suominen
Submitted for publication, arXiv:1304.4914 (2013) (6 pages).

IV *Efficient two-dimensional subrecoil Raman cooling of atoms in a tripod configuration*
V. S. Ivanov, Yu. V. Rozhdestvensky, and K.-A. Suominen
Physical Review A **83** (2011) 023407 (5 pages).

V *Robust two-dimensional subrecoil Raman cooling by adiabatic transfer in a tripod atomic system*
V. S. Ivanov, Yu. V. Rozhdestvensky, and K.-A. Suominen
Physical Review A **86** (2012) 033409 (7 pages).

Chapter 1

Introduction

The interaction of an atomic ensemble with external fields is of interest from both theoretical and experimental viewpoints. In last decades, advances in experiments have led to the observation of new sorts of atomic media such as Bose-Einstein condensate (BEC) [1], a single atom in a trap [2] and a quantum qubit [3, 4]. These experiments have opened new prospects of studying fundamental properties of atomic interaction in the condensed matter [5], ultracold particle collisions [6] and quantum entanglement [7–9]. Along with other reasons, this great success was initiated by the presence of atomic transitions driven by optical laser sources. This interaction has quantum nature which appears in such effects as electromagnetically induced transparency [10] and coherent population trapping [11, 12]. Stimulated widespread study of this interaction has made a considerable contribution in high-precision measurements [13–15], atomic clocks [16–18] and quantum computing [19, 20].

At the same time, it has turned out that managing intrinsic atomic levels yields an effective tool to manipulate extrinsic degrees of freedom not only of a charged particle but also of a neutral atom. Absorption or emission of a photon is accompanied by a momentum kick of $\hbar\mathbf{k}$ involving the acceleration or deceleration of the atom by resonant light of the wave vector $\mathbf{k}$, giving many possibilities of a high-precision control on atomic motion. This fact has found applications in high-precision measurements using absorbing masks of light [13, 14], atom nanolithography [15, 21], and optical trapping and cooling [22–24]. At the cost of additional tools, it has made possible obtaining BEC by means of evaporative cooling following optical cooling [25], as well as cooling other sorts of atoms via sympathetic cooling [26]. Laser cooling is also used in experiments with non-degenerate gases such as atomic clocks [27, 28] and ultraprecise measurements [17],

providing required large numbers of cold atoms.

A recoil momentum of $\hbar\mathbf{k}$ transferred by a photon to an atom characterizes the recoil-limit temperature $T_{\rm rec}$ of an atomic ensemble when the average velocity of atoms coincides with the recoil velocity $v_{\rm rec} = \hbar k/M$, where M is the atomic mass. Typical temperatures of cold atoms for cooling mechanisms based on continuous interaction with lasers are few times $T_{\rm rec}$. For instance, polarization gradient cooling [29–31] produces the mean velocity $v_{\rm rms}$ as low as $3{-}5v_{\rm rec}$. Going below the recoil limit became possible as proper cooling techniques were suggested. In 1988, Aspect and co-workers at the ENS in Paris demonstrated the possibility to cool atoms below the recoil limit by velocity-selective coherent population trapping (VSCPT) cooling [32]. A different subrecoil cooling scheme, namely, Raman cooling, was developed by Kasevich and Chu in 1992 at Stanford [33].

On the other hand, the development of atom-localization techniques [34–38] led to the overcoming of another fundamental limit connected to the Heisenberg's microscope [39]. Known from the early days of quantum mechanics, this tool imposes the limitation that the atomic position can not be detected more precise than the half-wavelength of radiation used for detection. With the development of localization methods affecting the internal atomic states, extremely high spatial resolutions of position measurement [34–36] and of state preparation [37, 38] were demonstrated. These techniques find important practical applications in neutral atom lithography with ultrahigh resolution [21].

For optical tools to be more efficient and powerful, the required atomic schemes become more complicated. For instance, a three-level Λ-type system suits fine for one-dimensional (1D) Raman cooling, for which the feasibility of deep subrecoil temperatures is confirmed in experiment [33]. Straightforward extensions to 2D and 3D were realized in Ref. [40], without the achievement of subrecoil temperatures. So far, experiments have demonstrated 2D Raman cooling down to $0.15T_{\rm rec}$ [41]. Hence, the use of a Λ-type scheme in 2D and 3D cases causes a crucial decrease in cooling efficiency. The main reason is the overall control on internal atomic states, which declines with the transfer to 2D and 3D. Situations are even more complicated, because the corresponding laser configurations may involve interactions with other sublevels of atomic hyperfine structure. These facts obviously show that the actual atomic scheme substantially affects on the success of techniques based on the atomic-level structure. Hence, finding and studying appropriate atomic schemes represents an additional issue, where most simple atomic schemes are preferred.

The use of powerful optical methods together with appropriate atomic schemes opens new opportunities and promising experiments, for instance, laser cooling of diatomic molecules [42] or fermionic isotopes [43, 44]. Also, new types of traps may be required, such as state-insensitive traps for precision metrology and quantum state engineering [17, 18, 45]. Not every technique realized in 1D can be extended to 2D and 3D cases, and thus it should pass a proper verification. As an example, a 3D scheme based on the $J = 1 \rightarrow J = 1$ configuration was suggested for VSCPT cooling [46], but has not found any application, because studied atomic states do not form a closed velocity family. At the same time, a transition from 1D to more dimensions usually introduces new aspects and features, unobservable in 1D. For instance, the extension of 1D atom localization [37, 38] to 2D (paper I) led to the discovering of three new spatial structures of population distribution such as spikes, craters, and waves.

The formulated issues stimulated us to search for an appropriate atomic scheme with further use in application to atom localization and subrecoil Raman cooling. In this thesis, we theoretically study a tripod-type atomic scheme [47, 48] attainable in metastable Ne, ^{87}Rb and other gases. The scheme is formed by a proper 2D laser configuration and represents a replacement of Λ-type scheme for 2D. In contrast to the $J = 1 \rightarrow J = 1$ configuration, the tripod-type linkage consists only of one upper and three ground states. In comparison with atom localization, subrecoil cooling puts higher demands of atomic system, where a dramatic role is played by the presence of long-living ground states and the capability of atomic states to form a closed velocity family. The tripod-type system fulfills both these requirements.

In the part devoted to 2D atom localization, the possibility to localize an atom within narrow domains substantially smaller than the optical wavelength is demonstrated (see also paper I), which opens new perspectives in the high-precision lithography with neutral atoms. The use of tripod-type scheme for 2D Raman cooling reduces the number of Raman beams down to three pairs (paper IV). Whereas the direct extension [40, 41] of the original Raman cooling to 2D requires four Raman beam pairs, producing temperatures down to $0.15T_{\rm rec}$ [41]. As shown in this thesis, tripod-type atoms in theory can be cooled down by an order of magnitude or even more, which means going down to $0.01T_{\rm rec}$. The scheme can also be used in transversal cooling of atomic beams, for example Ne* [47, 48]. However, 2D Raman cooling requires more cooling cycles as compared with 1D, imposing strict demands on the velocity precision of the Raman transfer. In other

words, one needs very accurate adjustment of laser detunings and the pulse area. We in turn suggest to overcome these limitations with the help of a STIRAP pulse which provides the robust transfer process (papers II, V). As a result, the cooling of tripod-type atoms down to $0.01T_{\mathrm{rec}}$ was achieved, which nevertheless allows a wide variation in both the pulse duration and envelope if only the adiabaticity criterion is satisfied. The pulse duration of STIRAP exceeds those of normal Raman processes, so the advantage of robustness is attained only if the cooling time is not in any critical role. This slowness related to adiabaticity would restrict the application of the method in atomic beam collimation to very slow beams. Because Raman cooling requires hundreds of cooling cycles to be applied, a natural question arises: Does the order of cycles influence the efficiency of cooling process? This thesis gives the answer in the part where an analytical form of the cold-atom momentum distribution is derived for the 1D case (paper III). It is shown that the resulting momentum distribution is independent of the cycle order once the number of applied cooling cycles is large enough.

The organization of this thesis is as follows. Chapter 2 considers the sub-wavelength localization of an atom in the field of resonant standing wave. Section 2.1 explains the principles of localization with an example of measuring spontaneous emission. This example, adapted in Sec. 2.2 to the 1D localization of an atom via its level population, finds practical applications in nanolithography [21]. Of greater interest is the 2D localization of a tripod-type atom via level population, which is presented in Sec. 2.3, classifying the upper-level population in respect to its 2D spatial structure. Chapter 3 gives a description of Raman cooling, starting from elementary cooling cycle in Sec. 3.1. Different mechanisms of coherent population transfer are discussed in Sec. 3.2. Section 3.3 presents the resulting cooling of an atomic ensemble, whose momentum distribution under certain conditions takes an analytical form, derived in Sec. 3.4. Section 3.5 extends Raman cooling over 2D, using a tripod-type atomic scheme. Finally, Chapter 4 concludes and summarizes the thesis.

Chapter 2

Atom localization

The prototype of an all-optical measuring device is the Heisenberg microscope [39], based on the uncertainty principle

$$\Delta p_x \Delta x \sim h. \tag{2.1}$$

The greatest momentum kick $\Delta p_x = 2\hbar k$, transferred from an optical photon to an atom, determines the precision of the atomic position measurement in terms of the optical wavelength λ:

$$\Delta x \sim \frac{\lambda}{2}. \tag{2.2}$$

Consequently, the Heisenberg microscope demonstrates that an atom can not be localized within the optical half-wavelength without involving the intrinsic atomic structure. Knowledge about the atomic-level structure initiated numerous localization techniques within a half-wavelength region, based on the measurement of the atomic resonance frequency [49–51], the phase shift [52–54] or the atomic dipole [55]. The highest localization degrees have been demonstrated by measuring either spontaneous emission [34–36] or a level population [37, 38] of an atom moving through a resonant standing wave.

2.1 Localization via spontaneous emission

The high-precision localization of an atom relies on position-dependent modification of its internal states. For this purpose, the atom passes through an optical standing wave inducing inhomogeneity within the optical half-wavelength. As shown in Fig. 2.1a, the atom is moving along the

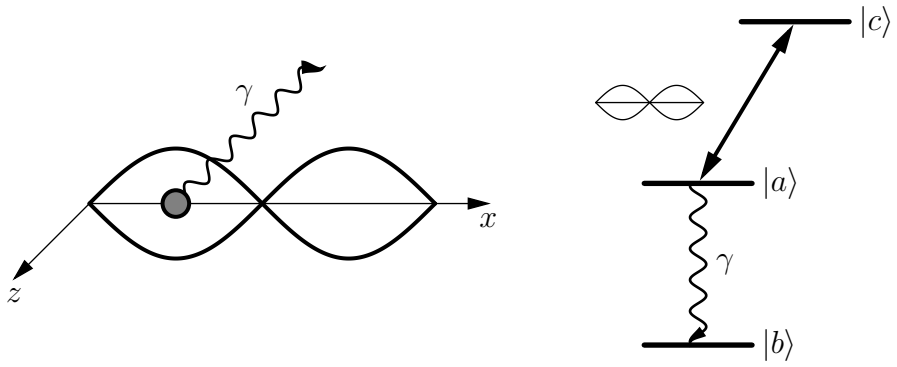

(a) (b)

Figure 2.1: An atom passes through a classical standing wave resonant to transition $|c\rangle \leftrightarrow |a\rangle$. The atom prepared in state $|a\rangle$ only decays through channel $|a\rangle \leftrightarrow |b\rangle$ with the decay rate γ. The standing-wave field creates an inhomogeneity along axis Ox, which allows to localize the atom after a spontaneously emitted photon is measured.

Oz direction, whereas the standing wave of wave vector $k = \omega/c$ is aligned along the Ox axis, and its electric field is given by

$$\mathbf{E}(\mathbf{r}, t) = \mathbf{E} \sin(kx) \cos(\omega t). \tag{2.3}$$

Assume that the atom has three levels, $|a\rangle$, $|b\rangle$, and $|c\rangle$, as shown in Fig. 2.1b, and the standing wave (2.3) is at the resonance with transition $|a\rangle \leftrightarrow |c\rangle$, i.e., $\omega = \omega_{ca}$. Incipient spontaneous radiation on transition $|a\rangle \leftrightarrow |b\rangle$ of the atom is detected during its motion through the standing wave. The center-of-mass deflection along axis Ox of the atom is considered to be negligible, which allows us to apply the Raman-Nath approximation and thus avoid the kinetic-energy term for the atom. The atomic Hamiltonian in the interaction representation and the rotating-wave approximation (RWA) is therefore written as [34]

$$\begin{aligned}\hat{H} = {} & \hbar g(x)\big(|c\rangle\langle a| + |a\rangle\langle c|\big) \\ & + \hbar \sum_{\mathbf{q}} \Big(g_{\mathbf{q}}(x) \exp(-i\delta_{\mathbf{q}} t) |a\rangle\langle b| \hat{b}_{\mathbf{q}} + g^*_{\mathbf{q}}(x) \exp(i\delta_{\mathbf{q}} t) |b\rangle\langle a| \hat{b}^\dagger_{\mathbf{q}} \Big). \end{aligned} \tag{2.4}$$

The coupling of transition $|a\rangle \leftrightarrow |c\rangle$ by the resonant standing wave is associated with the position-dependent Rabi frequency $g(x) = G \sin(kx)$, whereas the annihilation $\hat{b}_{\mathbf{q}}$ and creation $\hat{b}^\dagger_{\mathbf{q}}$ operators of photons with wave

vector $\mathbf{q}$ describe spontaneous emission through the $|a\rangle \leftrightarrow |b\rangle$ channel. A spontaneous photon emitted under the angle θ with respect to axis Ox has coupling parameter $g_{\mathbf{q}}(x) = G_{\mathbf{q}} \exp(iqx\cos\theta)$, where $q = |\mathbf{q}|$; $\delta_{\mathbf{q}} \equiv \nu_{\mathbf{q}} - \omega_{ab}$ is the detuning between the frequency $\nu_{\mathbf{q}} = cq$ of the photon and the frequency ω_{ab} of transition $|a\rangle \leftrightarrow |b\rangle$.

The atom-field state vector $|\Psi(t)\rangle$ of the atom is given by

$$|\Psi(t)\rangle = \int dx f(x)|x\rangle \Big(C_{a,0}(x;t)|a,0\rangle + C_{c,0}(x;t)|c,0\rangle + \sum_{\mathbf{q}} C_{b,1_{\mathbf{q}}}(x;t)|b,1_{\mathbf{q}}\rangle \Big). \quad (2.5)$$

Here, the position-dependent probability amplitudes $C_{i,0}(x;t)$ $(i = a, c)$ correspond to the atom in state $|i\rangle$ with no photons in the reservoir mode, whereas the probability amplitude $C_{b,1_{\mathbf{q}}}(x;t)$ describes the atom in ground level $|b\rangle$ and one photon in mode $\mathbf{q}$; $f(x)$ is the center-of-mass wave function of the atom.

The detector absorbs photons spontaneously emitted by the atom. A photon in mode $\mathbf{q}$ detected at time t allows us to determine the probability $W(x;t|b,1_{\mathbf{q}})$ for the atom to be at position x at the moment. The fact that the atom is found in state $|b,1_{\mathbf{q}}\rangle$ defines the reduced state of the atom,

$$|\psi^{(\mathrm{atom})}_{b,1_{\mathbf{q}}}\rangle = \mathcal{N}\langle b,1_{\mathbf{q}}|\Psi(t)\rangle = \mathcal{N}\int dx f(x) C_{b,1_{\mathbf{q}}}(x;t)|x\rangle, \quad (2.6)$$

where $\mathcal{N}$ is a normalization factor. Hence, the conditional position probability is given by

$$W(x;t|b,1_{\mathbf{q}}) = |\langle x|\psi^{(\mathrm{atom})}_{b,1_{\mathbf{q}}}\rangle|^2 = |\mathcal{F}(x;t|b,1_{\mathbf{q}})|^2 |f(x)|^2, \quad (2.7)$$

whose dependence on the probability amplitude $C_{b,1_{\mathbf{q}}}$ follows from the filter function

$$\mathcal{F}(x;t|b,1_{\mathbf{q}}) = |\mathcal{N}|^2 |C_{b,1_{\mathbf{q}}}(x;t)|^2. \quad (2.8)$$

The atomic Hamiltonian (2.4) and the probability function $|\Psi(t)\rangle$ (2.5) satisfy the Schrödinger equation

$$i\hbar \frac{\partial}{\partial t}|\Psi\rangle = \hat{H}|\Psi\rangle, \quad (2.9)$$

which in turn gives the following equations of motion for the probability amplitudes:

$$\dot{C}_{a,0} = -igC_{c,0} - i\sum_{\mathbf{q}} g_{\mathbf{q}} \exp(-i\delta_{\mathbf{q}} t) C_{b,1_{\mathbf{q}}}, \tag{2.10}$$

$$\dot{C}_{c,0} = -igC_{a,0}, \tag{2.11}$$

$$\dot{C}_{b,1_{\mathbf{q}}} = -ig^*_{\mathbf{q}} \exp(i\delta_{\mathbf{q}} t) C_{a,0}. \tag{2.12}$$

The formal solution of Eq. (2.12) with the initial condition $C_{b,1_{\mathbf{q}}}(t=0) = 0$ is written as

$$C_{b,1_{\mathbf{q}}} = -ig^*_{\mathbf{q}} \int_0^t dt' \exp(i\delta_{\mathbf{q}} t') C_{a,0}(t'). \tag{2.13}$$

Substituting the probability amplitude $C_{b,1_{\mathbf{q}}}$ (2.13) into Eq. (2.10) and applying the Weisskopf-Wigner approximation, one gets equation

$$\dot{C}_{a,0} = -igC_{c,0} - \gamma C_{a,0}, \tag{2.14}$$

where 2γ is the natural linewidth of level $|a\rangle$. Solving the reduced system of Eqs. (2.11) and (2.14), one gets decay from state $|a\rangle$. If the atom is originally prepared in the $|a\rangle$ state, then the probability amplitude $C_{a,0}$ is given by

$$C_{a,0}(x;t) = \exp(-\gamma t/2) \left(\cosh\{\tfrac{1}{2}[\gamma^2 - 4g^2(x)]^{1/2} t\} \right.$$
$$\left. - \frac{\gamma}{[\gamma^2 - 4g^2(x)]^{1/2}} \sinh\{\tfrac{1}{2}[\gamma^2 - 4g^2(x)]^{1/2} t\} \right). \tag{2.15}$$

The high-precision localization of the atom crucially depends on precision with which the frequency $\nu_{\mathbf{q}}$ of the spontaneously emitted photon is measured. The measurement with accuracy $|\Delta\nu_{\mathbf{q}}| \ll \gamma$ is possible for times considerably larger than the lifetime γ^{-1} of level $|a\rangle$, that is $\gamma t \gg 1$. In this long-time limit, we ensure that the photon is detected, and the probability amplitude $C_{b,1_{\mathbf{q}}}$ follows the steady-state solution

$$C_{b,1_{\mathbf{q}}}(x; t \to \infty) = -\frac{G^*_{\mathbf{q}} \exp(-ikx\cos\theta)\delta_{\mathbf{q}}}{G^2 \sin^2(kx) - \delta^2_{\mathbf{q}} - i\delta_{\mathbf{q}}\gamma}. \tag{2.16}$$

If we consider the coupling parameter $G_{\mathbf{q}}$ to be constant, then the filter function (2.8) is given by

$$\mathcal{F}(x; t \to \infty | b, 1_{\mathbf{q}}) \equiv \mathcal{F}(x) = |\mathcal{N}|^2 \frac{|G_{\mathbf{q}}|^2 \delta^2_{\mathbf{q}}}{[G^2 \sin^2(kx) - \delta^2_{\mathbf{q}}]^2 + \delta^2_{\mathbf{q}}}, \tag{2.17}$$

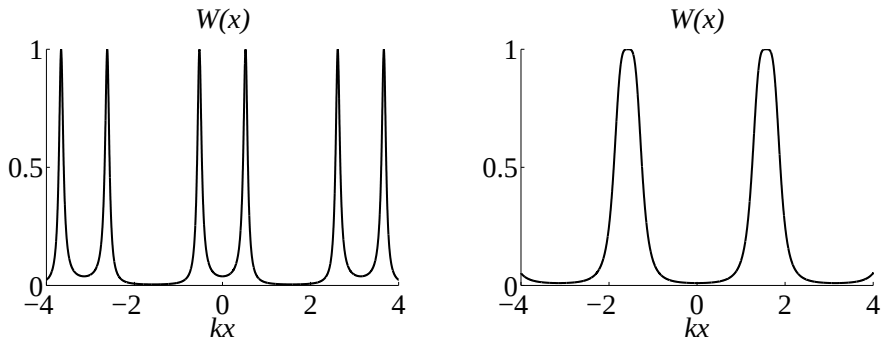

Figure 2.2: Conditional position distribution $W(x)$ (equation (2.7)) as a function of kx. The nodes of Rabi frequency $g(x)$ of amplitude $G = 10\gamma$ lie at positions $kx = 0, \pm\pi, \pm 2\pi, \ldots$. The peaks of $W(x)$ arise in a strong correlation with the detuning $\delta_{\mathbf{q}}$ of the measured spontaneously emitted photon. For $\delta_{\mathbf{q}} = 5\gamma$ (a) maxima lie between the antinode and node, and for $\delta_{\mathbf{q}} = 10\gamma$ (b) the positions of maxima approach antinodes. The peak positions are defined by the resonance condition $\delta_{\mathbf{q}} = G|\sin(kx)|$ following from Eq. (2.17).

and defines the conditional position distribution (2.7) in dependence on the frequency $\nu_{\mathbf{q}}$ of the spontaneously emitted photon.

Figure 2.2 shows the probability $W(x)$ of finding the atom at position x of an initially broad wave packet for two selected values of detuning $\delta_{\mathbf{q}} = \nu_{\mathbf{q}} - \omega_{ab}$, corresponding to the frequency $\nu_{\mathbf{q}}$ of the detected spontaneous photon. A strong correlation between the measured photon frequency $\nu_{\mathbf{q}}$ and the position x of the atom is reflected by the location of the maxima of $W(x)$, which strongly depends on the detuning $\delta_{\mathbf{q}}$. As a result, the atom is localized in a narrow position range within the half-wavelength of the standing wave.

Maxima in position distribution $W(x)$ defined by the frequency $\nu_{\mathbf{q}}$ of the spontaneously emitted photon are caused by the Autler-Townes effect [56, 57]. The maxima correspond to a doublet in the Autler-Townes spectrum, arising under the influence of a resonant wave on transition $|a\rangle \leftrightarrow |c\rangle$. The corresponding splitting between dressed states equals twice the Rabi frequency g, and the spectrum of spontaneous emission on transition $|a\rangle \leftrightarrow |b\rangle$ has two peaks at frequencies $\nu_{\mathbf{q}} = \omega_{ab} \pm g$. In our case, the fact that the Rabi frequency is position-dependent defines a strong correlation between the frequency of the spontaneously emitted photon and the position of the

atom within the half-wavelength domain.

2.2 Localization via level population

In the frame of the Raman-Nath approximation, the actual position distribution $f(x)$ of the atomic center-of-mass does not change during the measurement of a spontaneously emitted photon. In this case, the wave function $|\Psi\rangle$ of the atom does not provide information about the position of the atom in contrast to the reduced state $|\psi^{(\mathrm{atom})}_{b,1_\mathbf{q}}\rangle$. In other words, the assurance that the atom is found in state $|b, 1_\mathbf{q}\rangle$ after it emits the spontaneous photon allows us to localize the atom. However, we only probe the reduced wave function $|\psi^{(\mathrm{atom})}_{b,1_\mathbf{q}}\rangle$ without changing it. On the other hand, the possibility to manage a certain internal state would allow a high-precision technique to manipulate atoms localized in a narrow position range, not limited by the optical wavelength. There are demonstrations of several such techniques [37, 38] based on measuring population in an internal state, which may be applied for atom nanolithography [21] to form spatial structures of the order of few tens of nanometer on the sample surface.

Following closely Ref. [37, 38], we consider a three-level Λ-type atom shown in Fig. 2.3. A strong standing wave of frequency ω_1 couples transition $|1\rangle \leftrightarrow |2\rangle$, whereas a probe running wave of frequency ω_2 couples transition $|2\rangle \leftrightarrow |3\rangle$. Transition $|1\rangle \leftrightarrow |3\rangle$ is forbidden in the electric dipole approximation. Hence, the coupling operator $\hat{V}$ in the RWA and the interaction representation is written as

$$\hat{V} = \hbar g(x)\big\{|1\rangle\langle 2| + |2\rangle\langle 1|\big\} + \hbar\Omega\big\{|2\rangle\langle 3| + |3\rangle\langle 2|\big\}, \tag{2.18}$$

where $g(x) = G\sin(kx)$ is the position-dependent Rabi frequency of the standing-wave field, Ω is the constant Rabi frequency of the probe field. Assuming that the center-of-mass position of the atom along axis Ox does not change, we apply the Raman-Nath approximation and neglect the kinetic energy of the atom. Then, taking level $|1\rangle$ for the zero-energy floor, the atomic Hamiltonian is given by

$$\hat{H} = -\hbar\Delta_1|2\rangle\langle 2| + \hbar(\Delta_2 - \Delta_1)|3\rangle\langle 3| + \hat{V}, \tag{2.19}$$

where $\Delta_1 = \omega_1 - \omega_{21}$, $\Delta_2 = \omega_2 - \omega_{23}$ are the detunings from the upper state $|2\rangle$ to states $|1\rangle$ and $|3\rangle$, respectively.

Spontaneous decays through channels $|2\rangle \leftrightarrow |m\rangle$ $(m = 1, 3)$ with the decay rates γ_1 and γ_2, respectively, determine the natural linewidth $\gamma =$

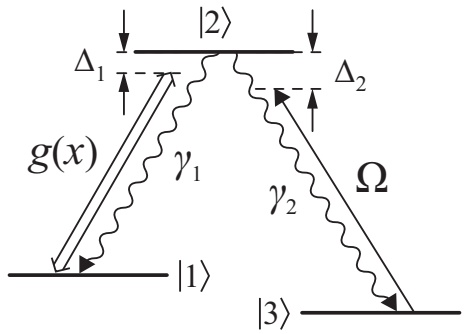

Figure 2.3: Population localization of a Λ-type atom. A spatial inhomogeneity of atomic populations follows from the position-dependent Rabi frequency $g(x)$ of standing wave coupling transition $|1\rangle \leftrightarrow |2\rangle$. The adjacent transition $|2\rangle \leftrightarrow |3\rangle$ of the atom is coupled by a probe field of Rabi frequency Ω. The detunings of the standing-wave and probe fields are Δ_1 and Δ_2, respectively; γ_1, γ_2 are the decay rates from the upper state.

$\gamma_1 + \gamma_2$ of the upper level $|2\rangle$. Spectral widths of optical transitions are $2\Gamma_{12}$ and $2\Gamma_{23}$. In order to take into account all the relaxation rates, we describe this localization scheme with the help of density matrix ρ, whose the equation of motion is given by [58]

$$i\hbar\frac{d}{dt}\rho = [\hat{H}, \rho] - i\hbar R(\rho), \tag{2.20}$$

with the atomic Hamiltonian (2.19) and the linear relaxation contribution $R(\rho)$ from the decay rates. Consequently, the equations of motion for the density-matrix elements ρ_{ij} are written as

$$i\dot{\rho}_{11} = -g(x)(\rho_{12} - \rho_{21}) + i\gamma_1\rho_{22}, \tag{2.21a}$$
$$i\dot{\rho}_{22} = g(x)(\rho_{12} - \rho_{21}) - \Omega(\rho_{23} - \rho_{32}) - i\gamma\rho_{22}, \tag{2.21b}$$
$$i\dot{\rho}_{33} = \Omega(\rho_{23} - \rho_{32}) + i\gamma_2\rho_{22}, \tag{2.21c}$$
$$i\dot{\rho}_{12} = -g(x)(\rho_{11} - \rho_{22}) - \Omega\rho_{13} + \Delta_1\rho_{12} - i\Gamma_{12}\rho_{12}, \tag{2.21d}$$
$$i\dot{\rho}_{13} = -\Omega\rho_{12} + g(x)\rho_{23} - (\Delta_2 - \Delta_1)\rho_{13}, \tag{2.21e}$$
$$i\dot{\rho}_{23} = \Omega(\rho_{33} - \rho_{22}) + g(x)\rho_{13} - \Delta_2\rho_{23} - i\Gamma_{23}\rho_{23}. \tag{2.21f}$$

The rest of equations for density-matrix elements follow from Eqs. (2.21) as their complex conjugates. Similarly to Sec. 2.1, the localization of the atom is considered in the long-time limit, when

$$\dot{\rho}_{ij} = 0, \quad i, j = 1, 2, 3. \tag{2.22}$$

The effect of coherent population trapping (CPT) in ground states $|1\rangle$ and $|3\rangle$ of a three-level Λ-type atom is observed in the case of equal detunings ($\Delta_1 = \Delta_2$). As follows from Eqs. (2.21) and (2.22), the atomic-level populations are then given by

$$\rho_{11} = \frac{\Omega^2}{g^2(x) + \Omega^2}, \quad \rho_{22} = 0, \quad \rho_{33} = \frac{g^2(x)}{g^2(x) + \Omega^2}. \tag{2.23}$$

The atom localization in the CPT case was considered by Agarwal and Kapale [21]. The case of the strong standing wave and the weak probe wave ($G \gg \Omega$) demonstrates the localization of the atom in state $|1\rangle$ near the node of the standing wave $g(x)$.

In the case of unequal detunings ($\Delta_1 \neq \Delta_2$), the spatial dependence of atomic populations has a more complex form in comparison with the CPT case. As follows from Appendix A, the steady-state solution of Eqs. (2.21) for the two-photon detuning $\delta \neq 0$, where $\delta = \Delta_2 - \Delta_1$, is written as

$$\rho_{11} = \frac{\Omega^2}{A}\left(2\Gamma_{12}\Gamma_{23}g^2(x) + \gamma_1 \operatorname{Re}(\beta\alpha_1)\right), \tag{2.24}$$

$$\rho_{22} = \frac{2\Gamma_{12}\Gamma_{23}g^2(x)\Omega^2}{A}, \tag{2.25}$$

$$\rho_{33} = \frac{g^2(x)}{A}\left(2\Gamma_{12}\Gamma_{23}\Omega^2 + \gamma_2 \operatorname{Re}(\beta\alpha_2)\right), \tag{2.26}$$

where the denominator is given by

$$A = 6\Gamma_{12}\Gamma_{23}g^2(x)\Omega^2 + \gamma_1\Omega^2 \operatorname{Re}(\beta\alpha_1) + \gamma_2 g^2(x) \operatorname{Re}(\beta\alpha_2), \tag{2.27}$$

and the rest of values are

$$\beta = \left(\Gamma_{12} - i\Delta_1 - i\frac{\Omega^2}{\delta}\right)\left(\Gamma_{23} + i\Delta_2 - i\frac{g^2(x)}{\delta}\right) + \frac{g^2(x)\Omega^2}{\delta^2}, \tag{2.28}$$

$$\alpha_1 = \Gamma_{12} + i\Delta_1 + i\frac{\zeta}{\gamma_1\delta}, \tag{2.29}$$

$$\alpha_2 = \Gamma_{23} - i\Delta_2 + i\frac{\zeta}{\gamma_2\delta}, \tag{2.30}$$

$$\zeta = \gamma_1\Omega^2 + \gamma_2 g^2(x). \tag{2.31}$$

In this case, the localization of the atom may occur beside the nodes of the standing wave $g(x)$. For instance, let us consider population in the

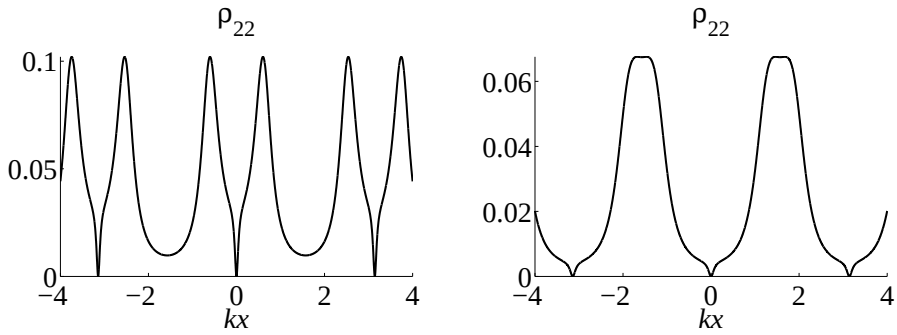

Figure 2.4: Spatial distribution of upper-state population ρ_{22} as a function of kx. The decay rates $\gamma_{1,2}$ from the upper state $|2\rangle$ are denoted as γ, the spectral widths $2\Gamma_{12}$, $2\Gamma_{23}$ of optical transitions $|2\rangle \leftrightarrow |m\rangle$ $(m = 1, 3)$ equal 2γ. The nodes of Rabi frequency $g(x)$ of amplitude $G = 3\gamma$ lie at positions $kx = 0, \pm\pi, \pm 2\pi, \ldots$, whereas the positions of maxima in spatial distribution ρ_{22} are defined by the detunings having the following values: (a) $\Delta_1 = 0.5\gamma$, $\Delta_2 = 2\gamma$; (b) $\Delta_1 = 4.5\gamma$, $\Delta_2 = 6\gamma$. The Rabi frequency Ω of the probe field equals 0.3γ.

upper state $|2\rangle$ for position x far from the nodes, where $g(x) \gg \Omega$. Hence, the spatial dependency of ρ_{22} is given by

$$\rho_{22}(x) \approx \frac{2\Omega^2}{\gamma_2} \frac{\Gamma_{23}}{\left(\Delta_2 - \dfrac{g^2(x)}{\delta}\right)^2 + \Gamma_{23}^2}. \tag{2.32}$$

Figure 2.4 illustrates the localization of the atom in the upper state $|2\rangle$ for detunings $\delta, \Delta_2 > 0$. In the case of $\delta\Delta_2 \ll G^2$, population ρ_{22} has two narrow symmetric peaks on the left and right of nodes $kx = 0, \pm\pi, \ldots$, as shown in Fig. 2.4a. As follows from Eq. (2.32), the positions of the peaks correspond to relationship

$$g^2(x) \approx \delta\Delta_2. \tag{2.33}$$

For instance, the positions of peaks around node $x = 0$ are given by

$$kx \approx \pm \arcsin\left(\frac{\sqrt{\delta\Delta_2}}{G}\right). \tag{2.34}$$

When the condition of $\delta\Delta_2 = G^2$ is satisfied, these peaks approach antinodes $kx = \pm\pi/2$ (see Fig. 2.4b).

The peaks in the spatial distribution of the upper-state population ρ_{22} can be explained in terms of the dressed-state picture. In this representation, levels $|1\rangle$ and $|2\rangle$ are split under the influence of the strong standing wave $g(x)$, where $g(x) \gg \Omega$. Taking into account that $\delta = \Delta_2 - \Delta_1$, we transform Eq. (2.33) to the following form:

$$\frac{\Delta_1 \pm \sqrt{4g^2(x) + \Delta_1^2}}{2} \approx \Delta_2. \tag{2.35}$$

Here, the left-hand side represents the splitting of the upper state $|2\rangle$, whereas the right-hand side ensures that probe field coupling transition $|2\rangle \leftrightarrow |3\rangle$ is tuned into resonance with a dressed state.

2.3 Two-dimensional localization via level population

The two-dimensional (2D) spatial localization of an atom in scales substantially smaller than an optical wavelength is of a great interest in atom nanolithography. Such a localization is achieved in the field of two perpendicular standing optical waves producing the mask of light [13, 14] and thus changing populations in atomic levels.

Let us consider the four-level tripod-type atom shown in Fig. 2.5a for the needs of atom localization as it was suggested in paper I. The atomic transition $|2\rangle \leftrightarrow |4\rangle$ is coupled by a linear-polarized standing-wave laser of the Rabi frequency $g_2(y) = G_2 \sin(ky)$ and the detuning Δ_2, which forms a position inhomogeneity along axis Oy (see Fig. 2.5b). Two lasers circular-polarized in opposite directions propagate along axis Ox and couple transitions $|1\rangle \leftrightarrow |4\rangle$ and $|3\rangle \leftrightarrow |4\rangle$ of the atom. The standing-wave laser near-resonant to the $|1\rangle \leftrightarrow |4\rangle$ transition has the Rabi frequency $g_1(x) = G_1 \sin(kx)$ and the detuning Δ_1, whereas the laser near-resonant to the $|3\rangle \leftrightarrow |4\rangle$ transition is a running wave of the Rabi frequency Ω and the detuning Δ_3. The decay rates though channels $|4\rangle \leftrightarrow |m\rangle$ $(m = 1, 2, 3)$ equal γ_1, γ_2, and γ_3, respectively. Thus, the natural linewidth of the upper state $|4\rangle$ is given by $\gamma = \gamma_1 + \gamma_2 + \gamma_3$. Spectral widths of optical transitions are Γ_{14}, Γ_{24} and Γ_{34}.

We describe the dynamics of internal states of the atom at position (x, y) by density matrix $\rho(x, y, t)$. The equations of motion for density-

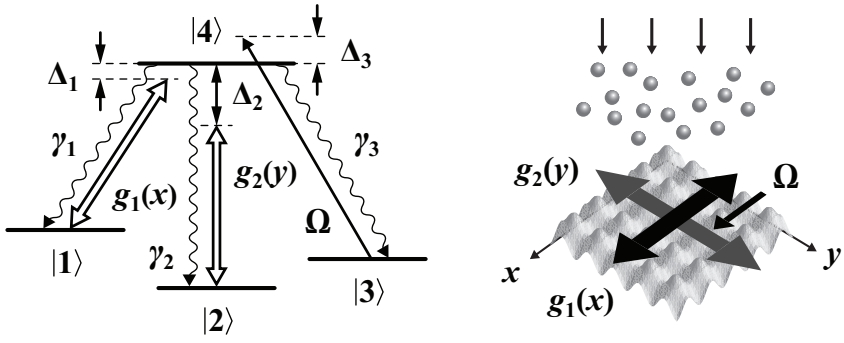

(a) (b)

Figure 2.5: A tripod-type atom falls along axis Oz and passes through a range of the interaction with two perpendicular strong standing waves of the Rabi frequencies $g_1(x)$ and $g_2(y)$, and a probe running wave of the Rabi frequency Ω. The waves propagating along axis Ox, $g(x)$ and Ω, are circularly polarized in opposite directions, and the linearly polarized wave $g(y)$ is aligned along axis Oy.

matrix elements are then given by

$$i\dot{\rho}_{11} = g_1(x)(\rho_{14} - \rho_{41}) + i\gamma_1\rho_{44}, \tag{2.36a}$$
$$i\dot{\rho}_{22} = g_2(y)(\rho_{24} - \rho_{42}) + i\gamma_2\rho_{44}, \tag{2.36b}$$
$$i\dot{\rho}_{33} = \Omega(\rho_{34} - \rho_{43}) + i\gamma_3\rho_{44}, \tag{2.36c}$$
$$i\dot{\rho}_{44} = g_1(x)(\rho_{41} - \rho_{14}) + g_2(y)(\rho_{42} - \rho_{24}) + \Omega(\rho_{43} - \rho_{34}) - i\gamma\rho_{44}, \tag{2.36d}$$
$$i\dot{\rho}_{12} = g_2(y)\rho_{14} - g_1(x)\rho_{42} + (\Delta_1 - \Delta_2)\rho_{12}, \tag{2.36e}$$
$$i\dot{\rho}_{13} = \Omega\rho_{14} - g_1(x)\rho_{43} + (\Delta_1 - \Delta_3)\rho_{13}, \tag{2.36f}$$
$$i\dot{\rho}_{23} = \Omega\rho_{24} - g_2(y)\rho_{43} + (\Delta_2 - \Delta_3)\rho_{23}, \tag{2.36g}$$
$$i\dot{\rho}_{14} = g_1(x)(\rho_{11} - \rho_{44}) + g_2(y)\rho_{12} + \Omega\rho_{13} + (\Delta_1 - i\Gamma_{14})\rho_{14}, \tag{2.36h}$$
$$i\dot{\rho}_{24} = g_2(y)(\rho_{22} - \rho_{44}) + g_1(x)\rho_{21} + \Omega\rho_{23} + (\Delta_2 - i\Gamma_{24})\rho_{24}, \tag{2.36i}$$
$$i\dot{\rho}_{34} = \Omega(\rho_{33} - \rho_{44}) + g_1(x)\rho_{31} + g_2(y)\rho_{32} + (\Delta_3 - i\Gamma_{34})\rho_{34}. \tag{2.36j}$$

The rest of equations for density-matrix elements follow from Eqs. (2.36) as their complex conjugates.

Similarly to Sec. 2.2, we consider the long-time limit ($\dot{\rho}_{ij} = 0$) and obtain the steady-state population ρ_{44} of the upper state $|4\rangle$ under the condition of weak probe field ($\Omega \ll g_1(x), g_2(y)$). In the case of $\Omega = 0$, strong standing waves $g_1(x)$, $g_2(y)$ displace all the atomic population into ground state $|3\rangle$, so that $\rho_{33} = 1$; the rest of density-matrix elements $\rho_{ij} = 0$.

These values of ρ_{ij} are considered as the starting approximation to the case of $\Omega \ll g_1(x), g_2(y)$. Consequently, Eqs. (2.36f) and (2.36g) give the steady-state density-matrix elements

$$\rho_{31} \approx \frac{g_1(x)}{\Delta_{13}}\rho_{34}, \quad \rho_{32} \approx \frac{g_2(y)}{\Delta_{23}}\rho_{34}, \tag{2.37}$$

where $\Delta_{13} = \Delta_1 - \Delta_3$, $\Delta_{23} = \Delta_2 - \Delta_3$. From Eq. (2.36j), it follows that

$$\rho_{34} \approx \frac{\Omega}{i\Gamma_{34} - \dfrac{g_1^2(x)}{\Delta_{13}} - \dfrac{g_2^2(y)}{\Delta_{23}} - \Delta_3}. \tag{2.38}$$

Here, the starting condition $\rho_{33} - \rho_{44} = 1$ is taken into account. Hence, Eq. (2.36c) gives the upper-state population in the form

$$\rho_{44} \approx -\frac{2\Omega^2}{\gamma_3}\,\mathrm{Im}\,\frac{1}{i\Gamma_{34} - \dfrac{g_1^2(x)}{\Delta_{13}} - \dfrac{g_2^2(y)}{\Delta_{23}} - \Delta_3}. \tag{2.39}$$

After the substitution of the explicit expression for the Rabi frequencies $g_1(x)$ and $g_2(y)$, the density-matrix element ρ_{44} is written as

$$\rho_{44} \approx \frac{2\Gamma_{34}\Omega^2}{\gamma_3 Z}, \tag{2.40}$$

where

$$Z = \left(\frac{G_1^2}{\Delta_{13}}\sin^2 kx + \frac{G_2^2}{\Delta_{23}}\sin^2 ky + \Delta_3\right)^2 + \Gamma_{34}^2. \tag{2.41}$$

Note that the form of the upper-state population given by (2.40) with (2.41) is similar to Eq. (2.32) obtained for a three-level Λ-type atom.

The upper-state population of the atom is given by Eqs. (2.40) and (2.41) for those atomic positions (x, y), where the condition of $\Omega \ll g_1(x), g_2(y)$ is satisfied. The situation becomes different when the atom passes the optical mask of light close to a nodal line of standing wave $g_1(x)$ or $g_2(y)$. The nodal-line position is defined by either $g_1(x) = 0$ or $g_2(y) = 0$, causing the atomic population in the long-time limit to be either in state $|1\rangle$ or $|2\rangle$, with no population in the upper state $|4\rangle$.

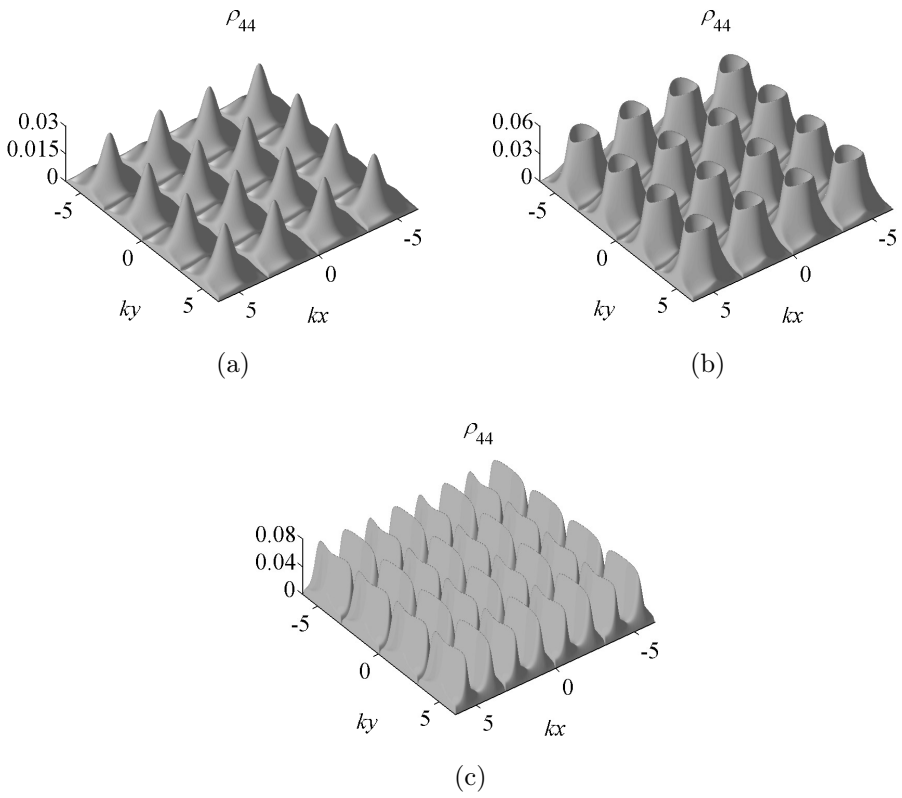

Figure 2.6: 2D periodic spatial structures of upper-state population ρ_{44} represent (a) spikes, (b) craters, and (c) waves. The kind of spatial structure is defined by the detunings having the following values: (a) $\Delta_1 = 10\gamma$, $\Delta_2 = 14\gamma$, $\Delta_3 = 16\gamma$; (b) $\Delta_1 = 5\gamma$, $\Delta_2 = 9\gamma$, $\Delta_3 = 11\gamma$; and (c) $\Delta_1 = \gamma$, $\Delta_2 = -3\gamma$, $\Delta_3 = 5\gamma$. Here, γ is the common decay rate through channels $|4\rangle \leftrightarrow |m\rangle$ $(m = 1, 2, 3)$, i.e, $\gamma_1, \gamma_2, \gamma_3 = \gamma$. The spectral widths of optical transitions, $2\Gamma_{14}$, $2\Gamma_{24}$, and $2\Gamma_{34}$, equal 2γ. The Rabi frequencies are $G_1 = 6\gamma$, $G_2 = 4\gamma$, and $\Omega = 0.3\gamma$.

2.3.1 Spatial structures of upper-level population

The spatial distributions of population in state $|4\rangle$ can be classified with the help of Eqs. (2.40) and (2.41). We select three types of spatial distribution such as spikes, craters, and waves, and illustrate them in Fig. 2.6, which in turn represents the result of numerical calculations for the long-time limit. Every population distribution forms a spatial periodic pattern with the minimal 2D domain of the size of $\lambda/2$, where λ is the optical wavelength.

As follows from Eq. (2.41), maxima of population ρ_{44} in the case of spikes occur at positions (x, y), where

$$\sin^2 kx \approx 1, \quad \sin^2 ky \approx 1, \tag{2.42}$$

which in turn gives the following positions of the maxima:

$$(x, y) \approx \Big((2m+1)\frac{\lambda}{4}, (2n+1)\frac{\lambda}{4}\Big), \tag{2.43}$$

with integer numbers m, n. Hence, population in the upper state shows how close to point (2.43) the atom passes the light mask, leading to the high-precision atom localization in the case of narrow spikes. In turn, the localization of the atom at a distance from point (2.43) is attained in the case of craters. One can see from Eq. (2.41) that the corresponding points of the maximal population are given by

$$\frac{G_1^2}{\Delta_{13}} \sin^2 kx + \frac{G_2^2}{\Delta_{23}} \sin^2 ky + \Delta_3 \approx 0. \tag{2.44}$$

Equation (2.44) defines the maximal population in the case of waves as well. For instance, parameters of the atom-field coupling may satisfy inequality

$$\left|G_2^2/\Delta_{23}\right| \ll \left|G_1^2/\Delta_{13}\right|. \tag{2.45}$$

In this case, Eq. (2.44) gives the following positions of the maximal population:

$$\sin^2 kx \approx \Delta_3(\Delta_3 - \Delta_1)/G_1^2. \tag{2.46}$$

As a result, the atom is localized along axis Ox. Also, the localization along axis Oy is possible, when

$$\left|G_1^2/\Delta_{13}\right| \ll \left|G_2^2/\Delta_{23}\right|. \tag{2.47}$$

The corresponding positions of the maximal upper-state population are given by

$$\sin^2 ky \approx \Delta_3(\Delta_3 - \Delta_2)/G_2^2. \tag{2.48}$$

The considered cases of spikes, craters and waves demonstrate that the localization of an atom in its upper state $|4\rangle$ is not limited by the optical wavelength λ, achieving spatial domains much smaller than λ^2. The precision of the localization increases together with the amplitudes G_1 and G_2

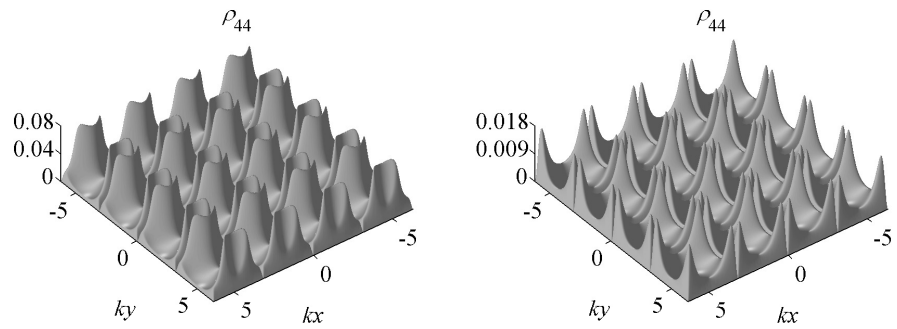

(a) (b)

Figure 2.7: 2D spatial structures from Fig. 2.6 shifted along directions Ox and Oy by $\lambda/4$, where $\lambda = 2\pi/k$ is the optical wavelength. (a) Craters after shifting along axis Oy to the nodal lines of standing wave $g_2(y)$; (b) spikes after shifting to the crossings of nodal lines of standing waves $g_1(x)$ and $g_2(y)$. The frequency detunings of lasers are (a) $\Delta_1 = -3\gamma$, $\Delta_2 = 5\gamma$, $\Delta_3 = 3\gamma$; and (b) $\Delta_1 = 8\gamma$, $\Delta_2 = 4\gamma$, $\Delta_3 = 2\gamma$. The other parameters of the atom-field coupling coincide with those in Fig. 2.6.

of the Rabi frequencies $g_1(x)$ and $g_2(y)$, whereas the intensity Ω^2 of the weak probe field defines the maximal value of the upper-state population.

The spatial structure of population distribution is defined by parameters of the atom-field coupling, which in turn can be adjusted to shift the structure along either the Ox or Oy axis by a spatial phase shift of $\pi/2$. It is straightforward to verify that transformations

$$\Delta_1' = 2\Delta_3 - \Delta_1 + G_1^2/\Delta_{13}, \tag{2.49a}$$
$$\Delta_2' = \Delta_2 + G_1^2/\Delta_{13}, \tag{2.49b}$$
$$\Delta_3' = \Delta_3 + G_1^2/\Delta_{13}, \tag{2.49c}$$

applied to denominator Z in Eq. (2.41), modify its value as

$$\begin{aligned} Z' &= \left(\frac{G_1^2}{\Delta_{13}'}\sin^2 kx + \frac{G_2^2}{\Delta_{23}'}\sin^2 ky + \Delta_3'\right)^2 + \Gamma_{34}^2 \\ &= \left(\frac{G_1^2}{\Delta_{13}}\sin^2\left(kx \pm \frac{\pi}{2}\right) + \frac{G_2^2}{\Delta_{23}}\sin^2 ky + \Delta_3\right)^2 + \Gamma_{34}^2. \end{aligned} \tag{2.50}$$

Whereas transformations

$$\Delta_1'' = \Delta_1 + G_2^2/\Delta_{23}, \tag{2.51a}$$
$$\Delta_2'' = 2\Delta_3 - \Delta_2 + G_2^2/\Delta_{23}, \tag{2.51b}$$
$$\Delta_3'' = \Delta_3 + G_2^2/\Delta_{23}, \tag{2.51c}$$

lead the denominator Z to the form

$$Z'' = \left(\frac{G_1^2}{\Delta_{13}}\sin^2 kx + \frac{G_2^2}{\Delta_{23}}\sin^2\left(ky \pm \frac{\pi}{2}\right) + \Delta_3\right)^2 + \Gamma_{34}^2. \tag{2.52}$$

New spatial structures determined by Eqs. (2.50) and (2.52) represent the original structure shifted along either the Ox or Oy axis by a spatial phase shift of $\pi/2$.

Figure 2.7 illustrates the result of applying the transformations (2.50) and (2.52) to such spatial structures as craters and spikes. Craters shifted along the Oy axis to the crossing with nodal lines of standing wave $g_2(y)$ are shown in Fig. 2.7a, whereas spikes shifted to the crossing of nodal lines of standing waves are shown in Fig. 2.7b.

Chapter 3

Raman cooling

After the discovering of VSCPT cooling in 1988 [32], Raman cooling [33] (1992) was the second technique which demonstrated cooling below the recoil limit. Both VSCPT and Raman cooling rely on a three-level Λ-type atomic system, but mechanisms used for the achievement of subrecoil temperatures are different. Raman cooling utilizes velocity-selective transfers among ground states in order to accumulate atoms in "dark states". Thereby, Raman cooling represents manipulating the internal degrees of freedom and accomplishes velocity selectivity in the same manner as the Maxwell's demon does. An improvement of internal-state manipulation reflects on the efficiency of Raman cooling, for instance, a qualitative analysis [59] given in the Lévy-flight approach [60] improved an earlier experiment [61] with a better fraction of atoms in the cold peak and a considerably simpler pulse sequence. The manipulation of internal atomic states extended over two and three dimensions made possible 2D and 3D Raman cooling as well [40, 41].

Temperatures archived by Raman cooling are substantially below the recoil limit, which in principle can not be reached by a cooling technique based on a continuous interaction of atoms with laser sources. In turn, Raman cooling originates from another cooling principle which can be explained in terms of a random walk in the velocity space. Each elementary cycle initiates such a random walk of an atom after a two-photon transfer and proceeding optical pumping. However, if the excitation profiles have the proper envelopes, atoms near the zero velocity remain untouched, i.e., these atoms stay in a "dark state". At that time, other atoms may fall into the dark state during the random walk, causing an accumulation of atoms near the zero velocity and cooling of the atomic ensemble. The final temperature is defined by the velocity width of the dark state, and reaches

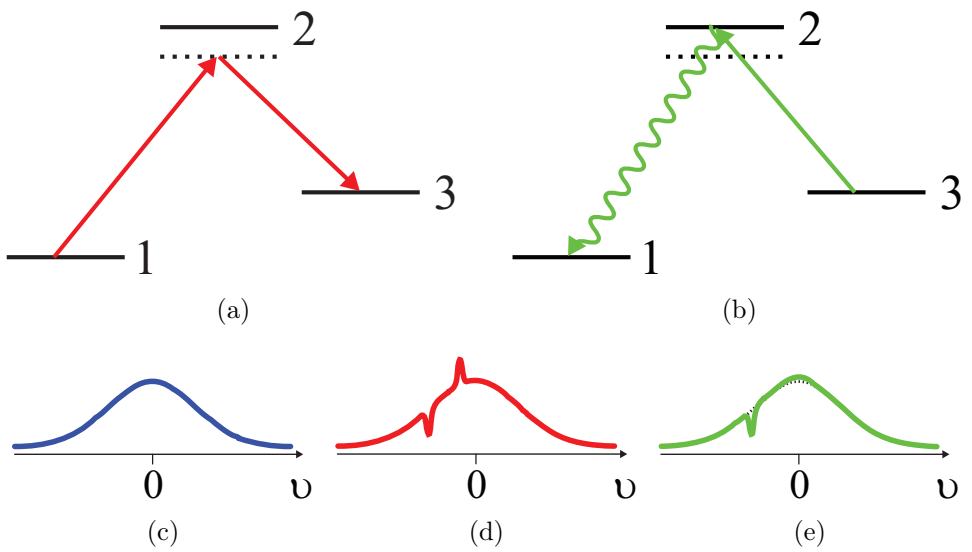

Figure 3.1: An elementary cycle of Raman cooling consists of (a) coherent population transfer and (b) optical pumping. (c) The initial Maxwell distribution of atoms which all seat in ground state $|1\rangle$. (d) and (e): velocity distributions after the first (a) and second (b) cooling steps. As a result, an increase of atoms near the zero velocity is observed.

very low values as the dark state becomes narrow.

3.1 Elementary cooling cycle

Raman cooling is a cyclical process, an elementary cycle of which is implemented in two steps shown in Fig. 3.1. We assume that the initial atomic ensemble, depicted in Fig. 3.1c, is Maxwell-distributed in velocity, and the atoms are in ground state $|1\rangle$. The first step of cooling cycle implements a transfer of atoms through two-photon resonance between states $|1\rangle$ and $|3\rangle$, created by two counter-propagating laser beams (see Fig. 3.1a). A certain velocity group of atoms is cut off and then transferred to adjacent ground state $|3\rangle$, forming a sharp population peak in the velocity distribution in Fig. 3.1d. This step realizes the concept of internal-state manipulation, determining where and how much atoms to be transferred. This step usually varies from cycle to cycle exciting different velocity groups of atoms in order to provide the most productivity. The second step shown in Fig. 3.1b is accomplished by optical pumping, returning all the atoms in ground state

$|3\rangle$ back to the original state $|1\rangle$. As a result, a growth in atoms around the zero velocity is observed (see Fig. 3.1e), involving a phase-space-density increase and cooling of the ensemble.

Raman cooling uses two laser beam configurations, which alternate during cooling process. For the first laser configuration, pump laser is aligned forwards the Oz axis and couples state $|1\rangle$ to the upper state $|2\rangle$, which in turn is coupled to state $|3\rangle$ by Stokes laser aligned backwards the Oz axis. As a result, atoms transferred in the first cooling step gain a momentum shift of $\hbar(\mathbf{k}_P - \mathbf{k}_S)$, where $\mathbf{k}_P = k\mathbf{e}_z$, $\mathbf{k}_S = -k\mathbf{e}_z$ are the wave vectors of the pump and Stokes lasers, respectively.

In the second step of cooling cycle, the pump laser is switched off, whereas the Stokes laser is tuned at the resonance and plays the role of optical pump, exciting atoms from state $|3\rangle$ to the upper state $|2\rangle$. An excited atom then decays through channel $|2\rangle \leftrightarrow |1\rangle$, when a spontaneously emitted photon of momentum $\Delta\mathbf{p}$ takes away a part of the atomic kinetic energy, causing a cooling of the atom. Hence, in the second cooling step, the atomic momentum is shifted by $\hbar\mathbf{k}_S - \Delta\mathbf{p}$, so that the total momentum shift after the cooling cycle (steps 1 and 2 combined) is given by

$$\delta\mathbf{p} = \hbar(\mathbf{k}_P - \mathbf{k}_S) + (\hbar\mathbf{k}_S - \Delta\mathbf{p}) \equiv \hbar\mathbf{k}_P - \Delta\mathbf{p}. \tag{3.1}$$

Because $|\Delta\mathbf{p}| \approx \hbar k$, the projection of $\delta\mathbf{p}$ on axis Oz is non-negative and, hence, the atom has been pushed in the velocity space forwards the Oz axis. If the atomic velocity before the cooling cycle was on the left-hand side of axis Oz, the atom experiences cooling.

The second laser configuration takes place when the pump laser propagates backwards the Oz axis ($\mathbf{k}_P = -k\mathbf{e}_z$), and the Stokes laser propagates forwards the Oz axis ($\mathbf{k}_S = k\mathbf{e}_z$). Under this laser configuration, an elementary cooling cycle in relation to the velocity space pushes atoms to the left against axis Oz and is used for cooling atoms on the right-hand side of the velocity distribution. Consequently, alternating the first and second laser beam configurations cool the atomic ensemble in total.

3.2 First step of cooling cycle

Let us consider the first step of cooling cycle applied for a three-level Λ-type atom shown in Fig. 3.2. The atom interacts with two lasers of frequencies ω_P, ω_S, resonant to transitions $|1\rangle \leftrightarrow |2\rangle$ and $|2\rangle \leftrightarrow |3\rangle$, respectively. The first laser configuration with $\mathbf{k}_P = k\mathbf{e}_z$, $\mathbf{k}_S = -k\mathbf{e}_z$, defines the following

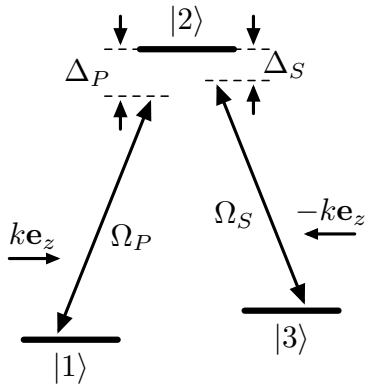

Figure 3.2: A three-level Λ-type atom interacts with the first laser beam configuration which includes a pump and Stokes lasers, near-resonant to transitions $|1\rangle \leftrightarrow |2\rangle$ and $|2\rangle \leftrightarrow |3\rangle$, respectively.

electric field:

$$\mathbf{E}(\mathbf{r},t) = \frac{1}{2}\mathbf{E}_P e^{ikz-i\omega_P t} + \frac{1}{2}\mathbf{E}_S e^{-ikz-i\omega_S t} + \text{c.c.} \tag{3.2}$$

To ensure that the one-photon resonances are avoided, we assume that

$$|\Delta_P| \gg \Gamma, |\Delta_S - \Delta_P|, \tag{3.3}$$

where $\Delta_P = \omega_P - \omega_{21}$, $\Delta_S = \omega_S - \omega_{23}$ are the detunings of the pump and Stokes laser, respectively; ω_{21}, ω_{23} are the frequencies of transitions $|1\rangle \leftrightarrow |2\rangle$ and $|2\rangle \leftrightarrow |3\rangle$; Γ is the natural linewidth of the upper state $|2\rangle$. As a result, decays through channels $|1\rangle \leftrightarrow |2\rangle$ and $|2\rangle \leftrightarrow |3\rangle$ are inhibited, and such a non-dissipative system is described by the Schrödinger equation

$$i\hbar\frac{\partial}{\partial t}|\Psi\rangle = \hat{H}|\Psi\rangle, \tag{3.4}$$

where $|\Psi\rangle$ is the probability function. The atomic Hamiltonian consists of the kinetic-energy term, the Hamiltonian of a non-moving atom with mass M, and the coupling operator:

$$\hat{H} = \frac{\hat{P}^2}{2M} + \hat{H}_0 + \hat{V}. \tag{3.5}$$

Taking the ground state $|1\rangle$ for the zero-energy floor of a non-moving atom, one gets

$$\hat{H}_0 = \hbar\omega_{21}|2\rangle\langle 2| + \hbar(\omega_{21} - \omega_{23})|3\rangle\langle 3|. \tag{3.6}$$

The interaction of the atom with the external laser fields is given by the coupling operator

$$\hat{V} = -\hat{\mathbf{d}}\mathbf{E}(\mathbf{r}, t), \tag{3.7}$$

where $\hat{\mathbf{d}}$ is the electric-dipole operator of the atom. The rotating-wave approximation (RWA) allows one to split up the coupling $\hat{V}$ into a sum of terms describing the coupling with transitions $|1\rangle \leftrightarrow |2\rangle$ and $|2\rangle \leftrightarrow |3\rangle$. Taking into account Eq. (3.2), the sum is written as

$$\hat{V} = -\frac{\mathbf{d}_{21}\mathbf{E}_P}{2}|2\rangle\langle 1|e^{ikz-i\omega_P t} - \frac{\mathbf{d}_{23}\mathbf{E}_S}{2}|2\rangle\langle 3|e^{-ikz-i\omega_S t} + \text{H.c.}, \tag{3.8}$$

where $\mathbf{d}_{21}$, $\mathbf{d}_{23}$ are the corresponding dipole moments; H.c. is the Hermitian conjugate. On the other hand, the strengths of laser couplings are defined by the corresponding Rabi frequencies,

$$\Omega_P = \left|\frac{\mathbf{d}_{21}\mathbf{E}_P}{\hbar}\right|, \quad \Omega_S = \left|\frac{\mathbf{d}_{23}\mathbf{E}_S}{\hbar}\right|, \tag{3.9}$$

which in turn allows, without loss of generality, to write the coupling operator $\hat{V}$ as

$$\hat{V} = \frac{\hbar\Omega_P}{2}|2\rangle\langle 1|e^{ikz-i\omega_P t} + \frac{\hbar\Omega_S}{2}|2\rangle\langle 3|e^{-ikz-i\omega_S t} + \text{H.c.} \tag{3.10}$$

Before a cooling cycle starts, an atom of a certain momentum projection p on axis Oz stays at state $|1, p\rangle$. Under the influence of the pump laser, the atom reaches the upper state $|2, p + \hbar k\rangle$; then it is transferred to the adjacent state $|3, p + 2\hbar k\rangle$ by the Stokes laser. These three states coupled by the first laser configuration form a closed momentum family

$$\mathcal{F}(p) = \{|1, p\rangle, |2, p + \hbar k\rangle, |3, p + 2\hbar k\rangle\}, \tag{3.11}$$

which provides a basis of states for the Schrödinger equation (3.4). As follows from (3.10), couplings between states of family $\mathcal{F}(p)$ are given by

$$\begin{aligned} \hat{V}|1, p\rangle &= \frac{\hbar\Omega_P}{2}e^{-i\omega_P t}|2, p + \hbar k\rangle, \\ \hat{V}|3, p + 2\hbar k\rangle &= \frac{\hbar\Omega_S}{2}e^{-i\omega_S t}|2, p + \hbar k\rangle, \end{aligned} \tag{3.12}$$

where the following relationships

$$e^{ikz} = \sum_p |p + \hbar k\rangle\langle p|, \quad e^{-ikz} = \sum_p |p + \hbar k\rangle\langle p + 2\hbar k|, \tag{3.13}$$

are taken into account. Using Eqs. (3.6) and (3.12), the atomic Hamiltonian (3.5) in the basis of $\mathcal{F}(p)$ is written as

$$\hat{H} = \hbar \begin{pmatrix} \dfrac{p^2}{2M\hbar} & \dfrac{1}{2}\Omega_P e^{i\omega_P t} & 0 \\ \dfrac{1}{2}\Omega_P e^{-i\omega_P t} & \dfrac{(p+\hbar k)^2}{2M\hbar} + \omega_{21} & \dfrac{1}{2}\Omega_S e^{-i\omega_S t} \\ 0 & \dfrac{1}{2}\Omega_S e^{i\omega_S t} & \dfrac{(p+2\hbar k)^2}{2M\hbar} + \omega_{21} - \omega_{23} \end{pmatrix}. \quad (3.14)$$

The interaction representation is given by states

$$|a_1\rangle = \exp\left\{-i\frac{p^2}{2M\hbar}t\right\}|1,p\rangle, \quad (3.15)$$

$$|a_2\rangle = \exp\left\{-i\left(\frac{p^2}{2M\hbar} + \omega_P\right)t\right\}|p+\hbar k\rangle, \quad (3.16)$$

$$|a_3\rangle = \exp\left\{-i\left(\frac{p^2}{2M\hbar} + \omega_P - \omega_S\right)t\right\}|3,p+2\hbar k\rangle, \quad (3.17)$$

in the basis of which the Hamiltonian (3.14) takes the form

$$\hat{H} = \hbar \begin{pmatrix} 0 & \dfrac{1}{2}\Omega_P & 0 \\ \dfrac{1}{2}\Omega_P & \dfrac{k(2p+\hbar k)}{2M} - \Delta_P & \dfrac{1}{2}\Omega_S \\ 0 & \dfrac{1}{2}\Omega_S & \dfrac{2k(p+\hbar k)}{M} + \Delta_S - \Delta_P \end{pmatrix}. \quad (3.18)$$

3.2.1 Population transfer by square pulse

The Hamiltonian (3.18) describes a non-dissipative Λ-type atomic system in general, including the case of a two-photon transfer from the $|1\rangle$ to $|3\rangle$ ground state. In the case of square pulse, the Rabi frequencies Ω_P, Ω_S are constant; the transfer has the simplest form for lasers of the same intensity:

$$\Omega_P = \Omega_S = \Omega. \quad (3.19)$$

In this symmetric case, the detuning from the $|3\rangle$ state of the Hamiltonian (3.18) in terms of the atomic velocity $v = p/M$ is written as

$$\frac{2k(p+\hbar k)}{M} + \Delta_S - \Delta_P = 2k(v - v_0). \quad (3.20)$$

Here, the two-photon resonant velocity v_0 corresponds to the zero detuning from the $|3\rangle$ state, i.e.,

$$2k(v_0 + v_{\rm rec}) + \Delta_S - \Delta_P = 0, \quad v_0 = \frac{\Delta_P - \Delta_S}{2k} - v_{\rm rec}, \tag{3.21}$$

where $v_{\rm rec} = \hbar k/M$ is the recoil velocity. Although Eq. (3.3) assumes detuning Δ_P to be large, the two-photon detuning $\Delta_S - \Delta_P$ in Eq. (3.21) can have as small values of the resonant velocity v_0 as needed for deep subrecoil cooling.

Atoms are only transferred by the two-photon resonance when

$$|\Delta_P| \gg \Gamma, |\Delta_S - \Delta_P|, k|v_0|, \omega_R, \tag{3.22}$$

where $\omega_R = \hbar k^2/(2M)$ is the recoil frequency. In addition, we assume that $\hbar\Delta_P$ exceeds largely the energy level splitting of the Λ-type atom,

$$|\Delta_P| \gg \Omega, \tag{3.23}$$

in order to adiabatically eliminate the upper state. Such elimination is possible when the probability function $|\Psi\rangle$ of atom in state $|2\rangle$ is approximately non-oscillatory:

$$\frac{d}{dt}\langle\Psi|a_2\rangle \approx 0. \tag{3.24}$$

In this case, the substitution of the Hamiltonian (3.18) into the Schrödinger equation (3.4) gives approximate equality

$$\langle\Psi|a_2\rangle \approx \frac{\Omega}{2\Delta_P}\big(\langle\Psi|a_1\rangle + \langle\Psi|a_3\rangle\big). \tag{3.25}$$

The adiabatic elimination and consequent relationship (3.25) reduce the Hamiltonian (3.18) to an effective Hamiltonian of a two-level system of states $|1\rangle$ and $|3\rangle$, describing population transfer between ground states of the original Λ-type system.

After the exclusion of state $|2\rangle$ from the Hamiltonian (3.18) with the help of Eq. (3.25), one gets the effective two-level Hamiltonian in the form

$$\hat{H}_{\rm eff} = \hbar \begin{pmatrix} -\delta_0 & \frac{1}{2}\Omega_{\rm eff} \\ \frac{1}{2}\Omega_{\rm eff} & 2k(v - v_0) - \delta_0 \end{pmatrix}, \tag{3.26}$$

where Eq. (3.20) is taken into account. The detuning and the Rabi frequency are given by

$$\delta_0 = -\frac{\Omega^2}{4\Delta_P}, \quad \Omega_{\text{eff}} = \frac{\Omega^2}{2\Delta_P}. \tag{3.27}$$

Once the intermediate state $|2\rangle$ is avoided, the atomic population is totally contained in the effective two-level system, i.e.,

$$|\langle\Psi|a_1\rangle|^2 + |\langle\Psi|a_3\rangle|^2 = 1, \tag{3.28}$$

where population transfer among states $|1\rangle$ and $|3\rangle$ is carried out by means of the two-photon Rabi frequency Ω_{eff}. Invoked Rabi oscillations in the effective system (3.26) give the following time dependence of populations in states $|1\rangle$ and $|3\rangle$:

$$\begin{aligned} |\langle\Psi|a_1\rangle|^2 &= 1 - \frac{\Omega_{\text{eff}}^2}{D_{\text{eff}}^2}\sin^2\left(\tfrac{1}{2}D_{\text{eff}}t\right), \\ |\langle\Psi|a_3\rangle|^2 &= \frac{\Omega_{\text{eff}}^2}{D_{\text{eff}}^2}\sin^2\left(\tfrac{1}{2}D_{\text{eff}}t\right), \end{aligned} \tag{3.29}$$

where

$$D_{\text{eff}} = \sqrt{\Omega_{\text{eff}}^2 + 4k^2(v - v_0)^2}. \tag{3.30}$$

The two-photon resonance $v = v_0$ corresponds to the greatest spread of Rabi oscillations, allowing the total population transfer from the $|1\rangle$ to $|3\rangle$ state, when the pulse duration T is given by

$$\Omega_{\text{eff}}T = \pi. \tag{3.31}$$

Condition (3.31) defines the Π-pulse which inverts the population of the effective two-level system. On the other hand, the zero velocity should be preserved from the transfer in order to accumulate atoms with $v = 0$. Using Eqs. (3.29) and (3.31), the corresponding relationship is written as

$$k|v_0|T = \frac{\sqrt{3}}{2}\pi. \tag{3.32}$$

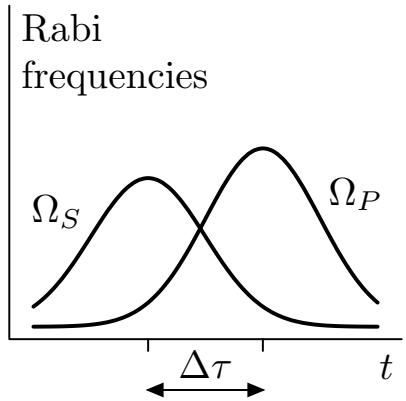

Figure 3.3: STIRAP pulse is formed by pump and Stokes pulses arranged in the counterintuitive order. The Gaussian profiles of pulses overlap during period $\Delta\tau$.

3.2.2 Population transfer by STIRAP

STIRAP is accomplished by the Gaussian pump and Stokes laser pulses arranged as in Fig. 3.3 in a counterintuitive order,

$$\Omega_P(t) = \Omega_{P0} e^{-(t-t_P)^2/2T_P^2}, \quad \Omega_S(t) = \Omega_{S0} e^{-(t-t_S)^2/2T_S^2}, \tag{3.33}$$

where $t_S < t_P$; $2T_P$, $2T_S$ are the pulse widths. These pulses transfer the resonant-velocity group of atoms from the original ground state $|1\rangle$ to state $|3\rangle$. The resonant velocity of the corresponding two-photon transition $|1\rangle \leftrightarrow |3\rangle$ is defined by the zero detuning from state $|3\rangle$ in the Hamiltonian (3.18). Hence, the resonant velocity of an atom prepared in state $|1\rangle$ is given by

$$v_0 = \frac{\Delta_P - \Delta_S}{2k} - v_{\mathrm{rec}}. \tag{3.34}$$

Under the resonant condition (3.34), the Hamiltonian (3.18) has the following basis of the time-dependent eigenstates (see Ref. [62, 63]):

$$|a^+\rangle = \sin\Theta \sin\Phi |a_1\rangle + \cos\Phi |a_2\rangle + \cos\Theta \sin\Phi |a_3\rangle, \tag{3.35a}$$
$$|a^0\rangle = \cos\Theta |a_1\rangle - \sin\Theta |a_3\rangle, \tag{3.35b}$$
$$|a^-\rangle = \sin\Theta \cos\Phi |a_1\rangle - \sin\Phi |a_2\rangle + \cos\Theta \cos\Phi |a_3\rangle. \tag{3.35c}$$

The time-dependent eigenvalues of the dressed states (3.35) are given by

$$\omega^{+} = \frac{1}{2}\left(\sqrt{\tilde{\Delta}_P^2 + \Omega_P^2(t) + \Omega_S^2(t)} - \tilde{\Delta}_P\right), \tag{3.36a}$$

$$\omega^{0} = 0, \tag{3.36b}$$

$$\omega^{-} = \frac{1}{2}\left(\sqrt{\tilde{\Delta}_P^2 + \Omega_P^2(t) + \Omega_S^2(t)} + \tilde{\Delta}_P\right), \tag{3.36c}$$

where $\tilde{\Delta}_P = \Delta_P + \omega_R - kp/M$. The angle Φ is determined by the detuning $\tilde{\Delta}_P$ and the Rabi frequencies [62]:

$$\tan\Phi = \frac{\sqrt{\Omega_P^2(t) + \Omega_S^2(t)}}{\sqrt{\tilde{\Delta}_P^2 + \Omega_P^2(t) + \Omega_S^2(t)} - \tilde{\Delta}_P}, \tag{3.37}$$

whereas the mixing angle Θ is a function of the Rabi frequencies only:

$$\tan\Theta = \frac{\Omega_P(t)}{\Omega_S(t)}. \tag{3.38}$$

Let us consider the case of large detuning Δ_P ($|\Delta_P| \gg \Omega_P(t), \Omega_S(t)$), leading to the reduced basis of the eigenstates equal to $\{|\mathrm{C}\rangle, |\mathrm{NC}\rangle, |a_2\rangle\}$. The coupled $|\mathrm{C}\rangle$ and non-coupled $|\mathrm{NC}\rangle$ states of the basis form the following linear combinations of ground states:

$$|\mathrm{C}\rangle = \sin\Theta|a_1\rangle + \cos\Theta|a_3\rangle, \tag{3.39a}$$

$$|\mathrm{NC}\rangle = \cos\Theta|a_1\rangle - \sin\Theta|a_3\rangle. \tag{3.39b}$$

Assuming that $|\Delta_P| \gg \omega_R, kp/M$, the corresponding eigenvalues are written as

$$\omega_{\mathrm{C}} = \frac{\Omega_P^2(t) + \Omega_S^2(t)}{4\Delta_P}, \quad \omega_{\mathrm{NC}} = 0. \tag{3.40}$$

The total population of atom is kept in states $|\mathrm{C}\rangle$ and $|\mathrm{NC}\rangle$, the interchange of population between these states is defined by the Hamiltonian matrix element $\langle \mathrm{C}|\frac{d}{dt}|\mathrm{NC}\rangle$ [64] for nonadiabatic coupling. The case, when this matrix element is much smaller than the energy splitting $|\omega_{\mathrm{C}} - \omega_{\mathrm{NC}}|$ induced by external fields, gives the "local" adiabaticity criterion:

$$|\langle \mathrm{C}|\frac{d}{dt}|\mathrm{NC}\rangle| \ll |\omega_{\mathrm{C}} - \omega_{\mathrm{NC}}|, \quad |\dot{\Theta}| \ll \frac{\Omega_P^2(t) + \Omega_S^2(t)}{4|\Delta_P|}. \tag{3.41}$$

The "global" adiabaticity criterion follows from Eq. (3.41) after the replacement of $\dot{\Theta}$ by its time-average value $\langle\dot{\Theta}_{av}\rangle = \pi/2\Delta\tau$:

$$\frac{\Omega_P^2(t) + \Omega_S^2(t)}{|\Delta_P|}\Delta\tau \gg 1, \tag{3.42}$$

where $\Delta\tau$ is the overlapping period of the pump and Stokes pulses.

The case of large detuning Δ_P ($|\Delta_P| \gg \Omega_P(t), \Omega_S(t)$) allows us to consider an atom with arbitrary velocity v and derive the velocity group of atoms transferred by STIRAP to state $|3\rangle$. As shown in Appendix B, if the adiabaticity criterion (3.42) is satisfied then this velocity group is given by

$$-\frac{\Omega_{S0}^2}{4k|\Delta_P|} < v - v_0 < \frac{\Omega_{P0}^2}{4k|\Delta_P|} \quad \text{if } \Delta_P > 0, \tag{3.43a}$$

$$-\frac{\Omega_{P0}^2}{4k|\Delta_P|} < v - v_0 < \frac{\Omega_{S0}^2}{4k|\Delta_P|} \quad \text{if } \Delta_P < 0. \tag{3.43b}$$

The obtained velocity range (3.43) only depends on the two-photon Rabi frequencies. The transfer probability grows from zero at a boundary of range (3.43) and reaches unity at the two-photon resonance.

During STIRAP pulse, intermediate state $|2\rangle$ is not occupied for the resonant atoms only. In other cases, population in the $|2\rangle$ state causes spontaneous decay to ground states $|1\rangle$ and $|3\rangle$ of the Λ-type atom. In order to estimate the contribution of the decay, we introduce the density operator σ, the matrix elements of which in the basis of states $|a_i\rangle$ ($i = 1, 2, 3$) are written as

$$\sigma_{ij}(p) = \langle a_i|\sigma|a_j\rangle, \quad i, j = 1, 2, 3. \tag{3.44}$$

Fraction of atoms spontaneously decaying from state $|2\rangle$ is defined by its natural linewidth Γ in accordance with equation

$$\frac{d}{dt}\sigma_{\rm sp}(p) = \Gamma\sigma_{22}(p). \tag{3.45}$$

We only consider the overlapping time $\Delta\tau$ of the pump and Stokes pulses when state $|2\rangle$ is actually populated. Hence the spontaneous-emission contribution is given by

$$\sigma_{\rm sp}(p) = \Gamma\int_0^{\Delta\tau}\sigma_{22}(p)dt. \tag{3.46}$$

The limitation on a portion of atoms in the upper state $|a_2\rangle$ follows from Eq. (B.1):

$$\sigma_{22}(p) \lesssim \frac{\Omega_P^2(t)}{2\Delta_P^2}\sigma_{11}(p) + \frac{\Omega_S^2(t)}{2\Delta_P^2}\sigma_{33}(p) \leq \frac{\Omega_P^2(t)+\Omega_S^2(t)}{2\Delta_P^2}. \tag{3.47}$$

This constraint on $\sigma_{22}(p)$ is then substituted into Eq. (3.46), giving the contribution

$$\sigma_{\rm sp}(p) \lesssim \Gamma\frac{\Omega_P^2(t)+\Omega_S^2(t)}{2\Delta_P^2}\Delta\tau. \tag{3.48}$$

Inequality $\sigma_{\rm sp}(p) \ll 1$ allows us to neglect from consideration spontaneous emission from state $|2\rangle$. Combining this inequality with the adiabaticity criterion (3.42) and Eq. (3.48), one gets condition

$$\frac{|\Delta_P|}{\Gamma} \gg \frac{\Omega_P^2(t)+\Omega_S^2(t)}{|\Delta_P|}\Delta\tau \gg 1, \tag{3.49}$$

which is satisfied when detuning Δ_P is large enough.

3.3 Cold-atom distribution

This Section shows the result of Raman cooling by STIRAP (see paper II for details). The cooling of atomic ensemble includes the alternation of the first and second laser beam configurations in order to cool whole the velocity distribution. Once the laser configuration is fixed, a sequence of cooling cycles is applied, so that a different velocity group of atoms is transferred in the beginning of each cycle. The left-hand side of the velocity distribution is cooled by transfer profiles shown in Fig. 3.4a. The broadest profile including atomic velocities far from the center of the distribution goes first, each next profile is narrower and closer to the center than the previous one. Such a cooling sequence passes through the left-hand side from the wing to the center, pushing atoms closer and closer to the zero velocity. However, the zero-velocity group is not excited, which in turn produces the accumulation of cold atoms there. The situation is repeated as the laser configuration is alternated. As a result, the atomic distribution is transformed into a narrow and high peak of cold atoms. The cooling process proceeds until the very low temperature is achieved.

The recoil temperature $T_{\rm rec}$ is defined by the velocity spread of the atomic ensemble,

$$\sigma = W_{\rm FWHM}/\sqrt{8\ln 2}, \tag{3.50}$$

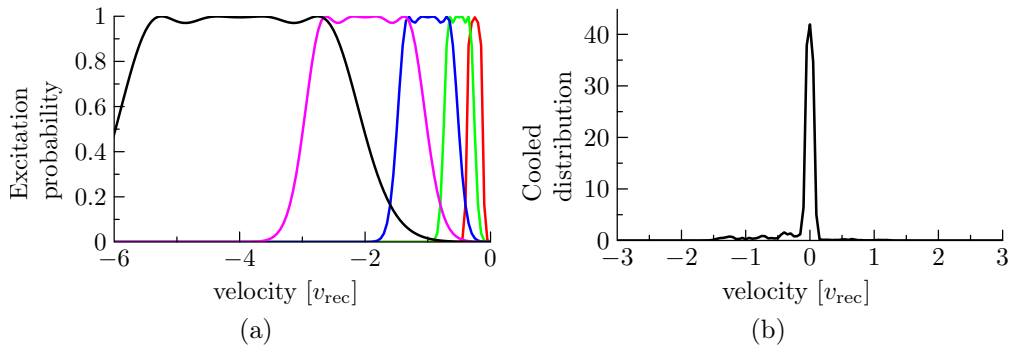

Figure 3.4: (a) The probability of transfer by STIRAP for different atom-field coupling parameters against the velocity v of atom in state $|1\rangle$. (b) The velocity distribution of cold atoms, the spread σ of the distribution has decreased from the initial $3v_{\mathrm{rec}}$ to $0.1v_{\mathrm{rec}}$.

equal to the one-photon recoil velocity ($v_{\mathrm{rec}} = \hbar k/M$). In general case, the temperature is given by

$$T = \left(\frac{\sigma}{\hbar k}\right)^2 T_{\mathrm{rec}}, \tag{3.51}$$

and declines as the squared velocity spread σ. Thereby, subrecoil Raman cooling requires a very narrow transfer profile of a small part of the recoil velocity v_{rec} to be attained. However, a Λ-type system contains a short-living upper state $|2\rangle$ capable to limit the resonant-velocity group by its natural linewidth Γ. That is why both lasers in the first step of cooling cycle are detuned from the one-photon resonances on values much larger than Γ in order to avoid such an undesirable broadening. In this case, the two-photon resonance is found far from the upper state which then is not occupied.

Figure 3.4b shows the velocity distribution after 200 cooling cycles of Raman cooling by STIRAP, starting from the initial distribution with the velocity spread of $3v_{\mathrm{rec}}$. The spread σ has been reduced to nearly $0.06v_{\mathrm{rec}}$, whereas the temperature of the atomic ensemble have gone down to $0.004T_{\mathrm{rec}}$.

3.4 Analytical form of momentum distribution

As seen in Sec. 3.3, Raman cooling down to subrecoil temperatures requires a large number of cooling cycles. So far, we got a cold-atom distribution by numerical calculations, and preliminarily studied only one cooling cycle. But such knowledge is not enough to understand properties of cold ensemble, requiring another approach which combines a large number of cooling cycles. Such a method allowing an arbitrary population transfer in the first step of cooling cycle was suggested in paper III.

Assume that a Λ-type atom of momentum $p = p_z$ is prepared in ground state $|1\rangle$ with the probability amplitude $a(p)$. As a cooling cycle starts, the atom is transferred to the adjacent ground state $|3\rangle$ through two-photon transition $|1\rangle \leftrightarrow |3\rangle$. The number of transferred atoms is given by

$$\Delta N = f(p)|a(p)|^2, \tag{3.52}$$

where $f(p)$ is the transfer probability. Consequently, the number of atoms left in state $|1\rangle$ is written as

$$|a_1(p)|^2 = (1 - f(p))|a(p)|^2. \tag{3.53}$$

Here, spontaneous emission from the upper state $|2\rangle$ is neglected, which becomes possible in the case of large the upper-state detuning as shown above in Subsecs. 3.2.1 and 3.2.2. As a result, atoms are only transferred by the two-photon transition $|1\rangle \leftrightarrow |3\rangle$, which in turn allows to deeply cool atoms because the momentum group of resonant atoms is not limited by the natural linewidth of the upper state.

In this general case, we do not specify laser beams, each of them may include one or more lasers, and only focus on the resulting probability $f(p)$ of population transfer. Independently to the number of lasers forming a laser beam, we describe it by the overall wave vector: pump laser near-resonant with transition $|1\rangle \leftrightarrow |2\rangle$ is described by $\mathbf{k}_P$, and Stokes laser near-resonant with transition $|2\rangle \leftrightarrow |3\rangle$ by $\mathbf{k}_S$. Raman cooling consists of two laser configurations: the first cools atoms with $p < 0$, and the second cools atoms with $p > 0$. Consequently, the first laser configuration is formed by $\mathbf{k}_P = k_P\mathbf{e}_z$, $\mathbf{k}_S = -k_S\mathbf{e}_z$, and the second one by $\mathbf{k}_P = -k_P\mathbf{e}_z$, $\mathbf{k}_S = k_S\mathbf{e}_z$. Hence, the transfer shifts the momentum of atom by $\pm\hbar(k_P+k_S)$ in respect to used laser beam configuration. As follows from Eq. (3.52), atoms in state $|3\rangle$ are given by

$$|a_3(p)|^2 = f(p \mp \hbar(k_P + k_S))|a(p \mp \hbar(k_P + k_S))|^2. \tag{3.54}$$

Here, the "−" and "+" signs are used for the first and second configuration of laser beams, respectively.

In the second step of cooling cycle, the pump laser is switched off, whereas the Stokes laser is tuned into resonance with transition $|2\rangle \leftrightarrow |3\rangle$. An atom of momentum p' in state $|3\rangle$ is excited to the upper state $|2\rangle$, gaining a momentum kick of $\hbar k_S$, so that its momentum becomes $p' \mp \hbar k_S$, where the sign of the kick depends on the laser beam configuration. Then the atom emits a spontaneous photon of momentum $\hbar k_P u$ and decays into state $|1\rangle$, when its momentum becomes $p = p' \mp \hbar k_S - \hbar k_P u$, where u is a random value within range $[-1, 1]$.

After this step, population distribution in state $|1\rangle$ is given by

$$|a'(p)|^2 = |a_1(p)|^2 + \int_{-1}^{1} N(u)|a_3(p \pm \hbar k_S + \hbar k_P u)|^2 du, \tag{3.55}$$

with the angular distribution $N(u)$ of spontaneously emitted photons. In turn, Eqs. (3.53) and (3.54) give the population change of the complete cooling cycle in the form

$$\begin{aligned} |a'(p)|^2 = {} & (1 - f(p))|a(p)|^2 \\ & + \int_{-1}^{1} N(u) f(p \mp \hbar k_P + \hbar k_P u)|a(p \mp \hbar k_P + \hbar k_P u)|^2 du. \end{aligned} \tag{3.56}$$

Although, in many cases Eq. (3.56) is the starting point for numerical calculations, paper III suggests a different way, taking the average of Eq. (3.56) over a large number of cooling cycles. Laser configurations alternate during cooling process, and the corresponding transfer probabilities $f(p)$ form sequences $F_1(p), \ldots, F_l(p)$ and $G_1(p), \ldots, G_l(p)$ for the first and second laser configuration, respectively; l is the number of different transfer envelops in each sequence. Once the average of Eq. (3.56) is obtained, we introduce the average transfer probabilities

$$F(p) = \frac{1}{l} \sum_{j=1}^{l} F_j(p), \quad G(p) = \frac{1}{l} \sum_{j=1}^{l} G_j(p). \tag{3.57}$$

The first laser configuration transfers atoms with $p < 0$, which in terms of $F(p)$ is written as

$$F(p) > 0, \quad \text{if } p < 0; \quad F(p) = 0, \quad \text{if } p \geq 0. \tag{3.58}$$

The corresponding relationship for the second laser configuration transferring atoms with $p > 0$ is given by

$$G(p) = 0, \quad \text{if } p \leq 0; \quad G(p) > 0, \quad \text{if } p > 0. \tag{3.59}$$

Note that Eqs. (3.58) and (3.59) correspond to the most efficient excitation profiles, accessible to STIRAP and Blackman [33, 40, 61] pulses, but not to square pulses.

In the assumption of Eqs. (3.58) and (3.59), the momentum distribution of atoms tends to the steady-state solution $\rho(p)$. Setting the scaling $\hbar k_P = 1$ in Eq. (3.56), paper III derives the following analytical expression:

$$\rho(p) = \begin{cases} 0, & p \leq -2; \\ \dfrac{A}{F(p)} \displaystyle\int_{-1-p}^{1} N(u)du, & p \in (-2, 0); \\ \dfrac{A}{G(p)} \displaystyle\int_{-1}^{1-p} N(u)du, & p \in (0, 2); \\ 0, & p \geq 2. \end{cases} \tag{3.60}$$

Here, the constant A is the normalization factor, the value of which follows from the fact that the number of atoms is conserved during the cooling process.

A specific case studied by the Levý-flight theory [60] corresponds to the Raman excitation spectrum (functions $F(p)$ and $G(p)$ with our notation) having the form of p^a, where $a > 0$. In turn, Eq. (3.60) divides this case into two parts: $a < 1$ and $a \geq 1$. One can see that the case of $a < 1$ is characterized by $A > 0$. On the other hand, the second case of $a \geq 1$ requires A to be equal to zero, so that the steady-state solution $\rho(p)$ equals zero for all momenta p except $p = 0$. In other words, the momentum distribution actually converges towards a delta function centered at $p = 0$. This fact is in a good agreement with the Levý flight theory, because, in both considerations efficient cooling takes place if $a \geq d$, where d is the dimensionality of cooling (here, $d = 1$).

3.5 Two-dimensional Raman cooling

In Sec. 3.2, we have considered a square pulse (Subsec. 3.2.1) and STIRAP (Subsec. 3.2.2) applied for coherent population transfer in the first cooling step; another possibility is the use of Blackman pulse [33, 40, 61]. In spite of differences between these pulses, Section 3.4 demonstrates that results of

1D Raman cooling can be approached in the same manner. The situation is different for 2D and 3D Raman cooling, where cold-atom distribution may vary if different pulse envelops are utilized. Although square pulses lead to efficient 2D cooling [59], Blackman pulses may be preferable in 3D, as predicted by the Levý-flight approach [60]. Notice that situations in 2D and 3D are not as successful as that in 1D, through the lack of simple atomic systems. On one hand, such a multidimensional cooling requires complicated experimental equipment, for instance, including four and eight Raman-beam pairs in 2D and 3D configurations, respectively [40]. On the other hand, the cooling efficiency is rather low, and even subrecoil 3D Raman cooling has not been demonstrated yet. The lowest temperature of 2D Raman cooling achieved in experiment is $0.15T_{\rm rec}$ [41]. As a possible path, papers IV and V suggest efficient 2D Raman cooling based on a tripod-type system attainable in ^{87}Rb, metastable Ne and other sorts of atoms. In this Section, we focus on cooling by STIRAP only (paper V), giving required additional notes for cooling by square pulses (paper IV).

3.5.1 Tripod-type system and laser configuration

Let us consider a four-level tripod-type system, using metastable Ne in Ref. [47] as an example. State $(2p^5 3s)\ ^3P_0$ is coupled by pump laser to an upper state $(2p^5 3p)\ ^3P_1$ $(M = 0)$, which in turn is coupled by two Stokes lasers to magnetic substates $M = \pm 1$ of $(2p^5 3s)\ ^3P_2$. The laser beam configuration is shown in Fig. 3.5a, where the π-polarized pump laser propagates along axis Oy, and the σ-polarized Stokes lasers propagate along axis Oz in opposite directions. The electric field of the laser configuration is written as

$$\mathbf{E}(\mathbf{r},t) = \frac{1}{2}\mathbf{E}_P e^{i\mathbf{k}_P\mathbf{r}-i\omega_P t} + \frac{1}{2}\mathbf{E}_S^+ e^{i\mathbf{k}_S\mathbf{r}-i\omega_S^+ t} + \frac{1}{2}\mathbf{E}_S^- e^{-i\mathbf{k}_S\mathbf{r}-i\omega_S^- t} + \text{c.c.} \quad (3.61)$$

The first term describes the pump laser of frequency ω_P and wave vector $\mathbf{k}_P = k_P\mathbf{e}_y$; two other terms describe the σ^+- and σ^--polarized Stokes lasers of frequencies ω_S^+, ω_S^- and wave vectors $\mathbf{k}_S$, $-\mathbf{k}_S$, respectively, where $\mathbf{k}_S = k_S\mathbf{e}_z$.

The atomic states coupled by the laser beam configuration are shown

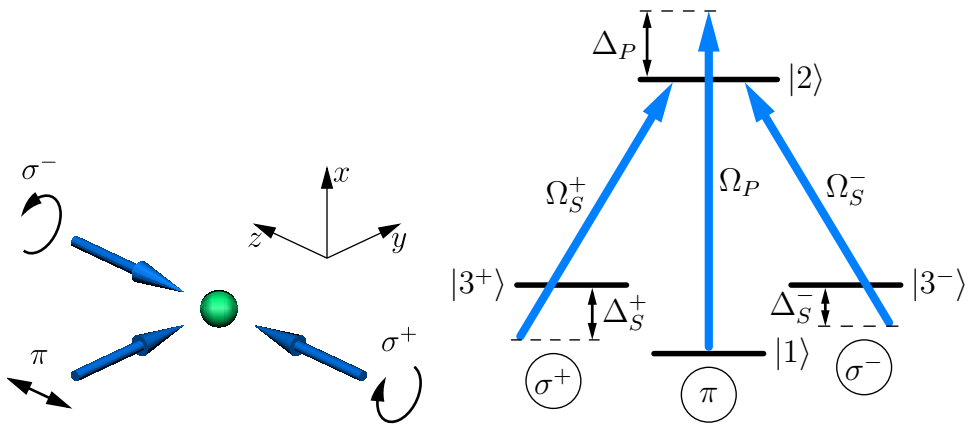

Figure 3.5: The 2D laser configuration includes three running waves: a π-polarized pump laser propagates in the Oy direction, and two σ-polarized Stokes lasers are arranged along axis Oz in opposite directions. (b) The atom-field coupling of a tripod-type system.

in Fig. 3.5b, with labelling

$$\begin{aligned}
|1\rangle &= |(2p^5 3s)\ {}^3P_0, M=0\rangle, \\
|2\rangle &= |(2p^5 3p)\ {}^3P_1, M=0\rangle, \\
|3^+\rangle &= |(2p^5 3s)\ {}^3P_2, M=-1\rangle, \\
|3^-\rangle &= |(2p^5 3s)\ {}^3P_2, M=1\rangle.
\end{aligned} \tag{3.62}$$

Originally, an atom is prepared in state $|1, \mathbf{p}\rangle$, where $\mathbf{p}$ is the atomic momentum. In the rotating wave approximation (RWA), the strengths of laser-atom coupling are written as

$$\begin{aligned}
\hat{V}|1, \mathbf{p}\rangle &= \frac{\hbar}{2}\Omega_P(t)e^{-i\omega_P t}|2, \mathbf{p}+\hbar\mathbf{k}_P\rangle, \\
\hat{V}|3^{\pm}, \mathbf{p}+\hbar\mathbf{k}_P \mp \hbar\mathbf{k}_S\rangle &= \frac{\hbar}{2}\Omega_S^{\pm}(t)e^{-i\omega_S^{\pm} t}|2, \mathbf{p}+\hbar\mathbf{k}_P\rangle.
\end{aligned} \tag{3.63}$$

Here, $\hat{V}$ is the coupling operator, and real-valued the Rabi frequencies are given by

$$\Omega_P(t) = -\frac{\mathbf{d}_{21}\mathbf{E}_P}{\hbar}, \quad \Omega_S^{\pm}(t) = -\frac{\mathbf{d}_{23}^{\pm}\mathbf{E}_S^{\pm}}{\hbar}, \tag{3.64}$$

where $\mathbf{d}_{21}$, $\mathbf{d}_{23}^{\pm}$ are the non-diagonal matrix elements of the dipole moment operator. In addition to the operator $\hat{V}$ of atom-field coupling, the atomic Hamiltonian

$$\hat{H} = \hat{H}_0 + \frac{\hat{\mathbf{P}}^2}{2M} + \hat{V} \tag{3.65}$$

includes the kinetic-energy term $\hat{\mathbf{P}}^2/(2M)$, and the Hamiltonian $\hat{H}_0$ of a non-moving atom having the internal level energies E_1, E_2, E_3^+ and E_3^-.

The contribution of spontaneous emission into population transfer is neglected in the case of large the upper-level detuning. The corresponding condition on the parameters of atom-field coupling is given in paper IV for square pulses (equation (6)) and in paper V for STIRAP (equation (13)). With spontaneous emission neglected, atomic states occupied by a tripod-type atom form a closed family of momentum $\mathbf{p}$:

$$\begin{aligned}\mathcal{F}(\mathbf{p}) = \{&|1,\mathbf{p}\rangle, |2,\mathbf{p}+\hbar\mathbf{k}_P\rangle,\\ &|3^+,\mathbf{p}+\hbar\mathbf{k}_P-\hbar\mathbf{k}_S\rangle, |3^-,\mathbf{p}+\hbar\mathbf{k}_P+\hbar\mathbf{k}_S\rangle\}.\end{aligned} \tag{3.66}$$

Then, in the representation of four bare states

$$\begin{aligned}|a_1\rangle &= \exp\left[-i\left(\frac{E_1}{\hbar}+\frac{\mathbf{p}^2}{2M\hbar}\right)t\right]|1,\mathbf{p}\rangle,\\ |a_2\rangle &= \exp\left[-i\left(\frac{E_2}{\hbar}+\frac{\mathbf{p}^2}{2M\hbar}+\Delta_P\right)t\right]|2,\mathbf{p}+\hbar\mathbf{k}_P\rangle,\\ |a_3^{\pm}\rangle &= \exp\left[-i\left(\frac{E_3^{\pm}}{\hbar}+\frac{\mathbf{p}^2}{2M\hbar}+\Delta_P-\Delta_S^{\pm}\right)t\right]\\ &\quad\times|3^{\pm},\mathbf{p}+\hbar\mathbf{k}_P\mp\hbar\mathbf{k}_S\rangle,\end{aligned} \tag{3.67}$$

the atomic Hamiltonian (3.65) is written as

$$H = \frac{\hbar}{2}\begin{pmatrix} 0 & \Omega_P(t) & 0 & 0\\ \Omega_P(t) & -2\tilde{\Delta}_P & \Omega_S^+(t) & \Omega_S^-(t)\\ 0 & \Omega_S^+(t) & 2\delta_S^+ & 0\\ 0 & \Omega_S^-(t) & 0 & 2\delta_S^- \end{pmatrix}, \tag{3.68}$$

where frequency detunings are given by

$$\begin{aligned}\tilde{\Delta}_P &= \Delta_P - \frac{k_P p_y}{M} - \omega_P^R,\\ \delta_S^{\pm} &= \Delta_S^{\pm} - \Delta_P + \frac{k_P p_y \mp k_S p_z}{M} + \omega_P^R + \omega_S^R.\end{aligned} \tag{3.69}$$

Here, p_y, p_z are projections on axes Oy and Oz of momentum $\mathbf{p}$, respectively; $\Delta_P = \omega_P - \omega_{21}$, $\Delta_S^{\pm} = \omega_S^{\pm} - \omega_{23}^{\pm}$ are the laser detunings; ω_{21}, $\omega_{23}^{\pm}$ are the atomic-transition frequencies; $\omega_P^R = \hbar k_P^2/(2M)$, $\omega_S^R = \hbar k_S^2/(2M)$ are the one-photon recoil frequencies.

3.5.2 Cooling mechanism

The velocity selectivity of population transfer in the first cooling step follows from the fact that velocities of atoms transferred by STIRAP correspond to dark state formed by ground states of the tripod-type system. Because the dark state is a combination of ground state $|1\rangle$ with either state $|3^+\rangle$ or $|3^-\rangle$, it occurs when two selected ground states satisfy the condition of two-photon resonance. As follows from the atomic Hamiltonian (3.68), the corresponding resonant velocities are given by

$$\delta_S^+ = 0 \quad \text{or} \quad \delta_S^- = 0. \tag{3.70}$$

The former condition is associated with population transfer through Raman transition $|1\rangle \leftrightarrow |3^+\rangle$, the latter is associated with transition $|1\rangle \leftrightarrow |3^-\rangle$.

Figures 3.6a and 3.6b illustrate velocities of atoms transferred to states $|3^+\rangle$ and $|3^-\rangle$, respectively; these velocity groups correspond to a hole burning for atoms in state $|1\rangle$, as shown in Fig. 3.6c. The transfer of dark-state atoms by two Raman transitions represents an obvious advantage of cooling in a tripod-type system, because atoms are cooled in two directions simultaneously. The laser beam configuration defines the burned cross-like hole in state $|1\rangle$, allowing one to vary only the hole position. The center of the cross-like pattern is given by

$$\delta_S^+ = \delta_S^- = 0, \tag{3.71}$$

and its position changes together with frequency detunings Δ_P, $\Delta_S^{\pm}$. Note that population transfer by a square pulse has a very similar picture of velocity selectivity (see Fig. 2 in paper IV). Although the position of cross-like hole is different, it is shifted by changing detunings Δ_P, $\Delta_S^{\pm}$ as well.

In the second cooling step, atoms from states $|3^+\rangle$ and $|3^-\rangle$ return to the original state $|1\rangle$ by means of optical pumping. For this purpose, the π-polarized pump laser is switched off, and the σ-polarized Stokes lasers are tuned into resonance with the corresponding one-photon transitions. An atom excited to the upper state $|2\rangle$ from either state $|3^+\rangle$ or $|3^-\rangle$ gains a momentum kick along axis Oz. As a result, the atomic momentum changes

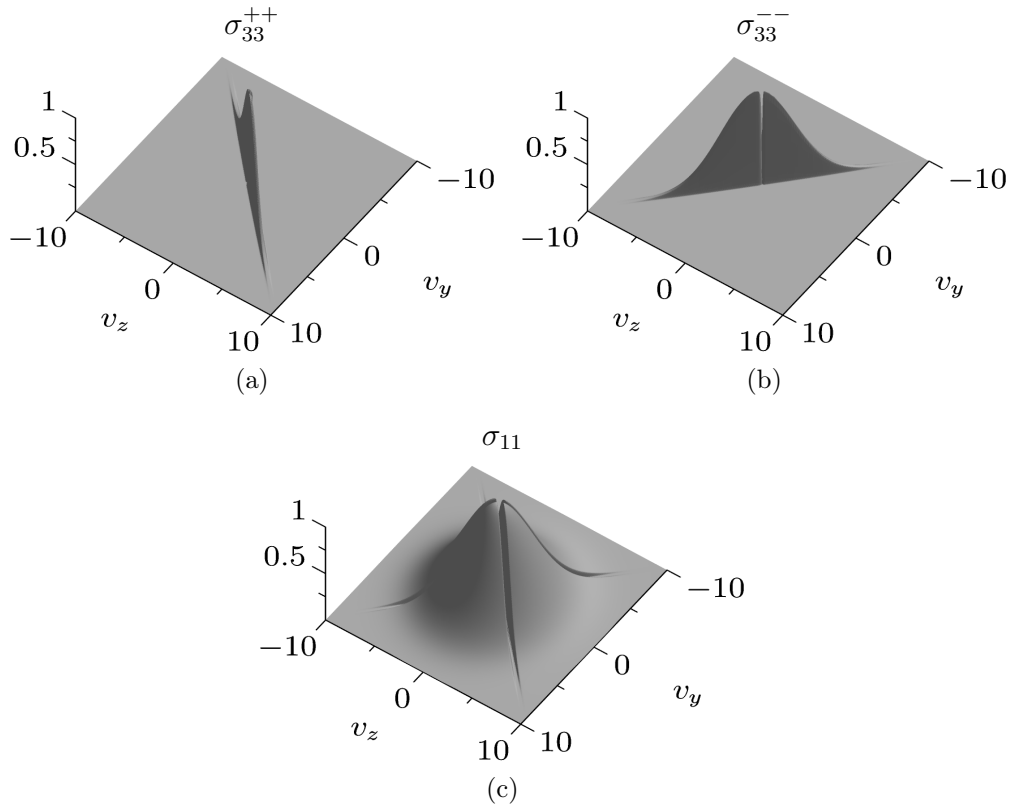

Figure 3.6: (a) and (b): Velocity groups of the initial distribution transferred by STIRAP into the $|3^+\rangle$ and $|3^-\rangle$ states, respectively. (c) The corresponding hole showing the depletion of atoms in state $|1\rangle$ due to these transfers. The scaling is given by the recoil velocity $v_{\rm rec} = \hbar k_P/M = \hbar k_S/M$.

from $\mathbf{p}$ to $\mathbf{p}' = \mathbf{p} \pm \hbar\mathbf{k}_S$, the sign of change corresponds to Stokes laser exciting the atom. Then the atom emits a spontaneous photon of momentum $\Delta\mathbf{p}$, where $|\Delta\mathbf{p}| \approx \hbar k_P$, and decays into state $|1\rangle$, gaining a momentum kick of $-\Delta\mathbf{p}$. Hence, after the cooling cycle finishes, population in state $|1\rangle$ is given by

$$\begin{aligned}\langle 1,\mathbf{p}|\hat{\sigma}'|1,\mathbf{p}\rangle = \langle 1,\mathbf{p}|\hat{\sigma}|1,\mathbf{p}\rangle + \langle 3^+,\mathbf{p}-\hbar\mathbf{k}_S+\Delta\mathbf{p}'|\hat{\sigma}|3^+,\mathbf{p}-\hbar\mathbf{k}_S+\Delta\mathbf{p}'\rangle \\ + \langle 3^-,\mathbf{p}+\hbar\mathbf{k}_S+\Delta\mathbf{p}''|\hat{\sigma}|3^-,\mathbf{p}+\hbar\mathbf{k}_S+\Delta\mathbf{p}''\rangle, \quad (3.72)\end{aligned}$$

where $\hat{\sigma}$ is the density operator. Let us introduce the density matrix elements corresponding to the momentum family $\mathcal{F}(\mathbf{p})$ (3.66):

$$\sigma_{ij}(\mathbf{p}) = \langle a_i|\hat{\sigma}|a_j\rangle, \quad i,j = 1,2,3^+,3^-. \quad (3.73)$$

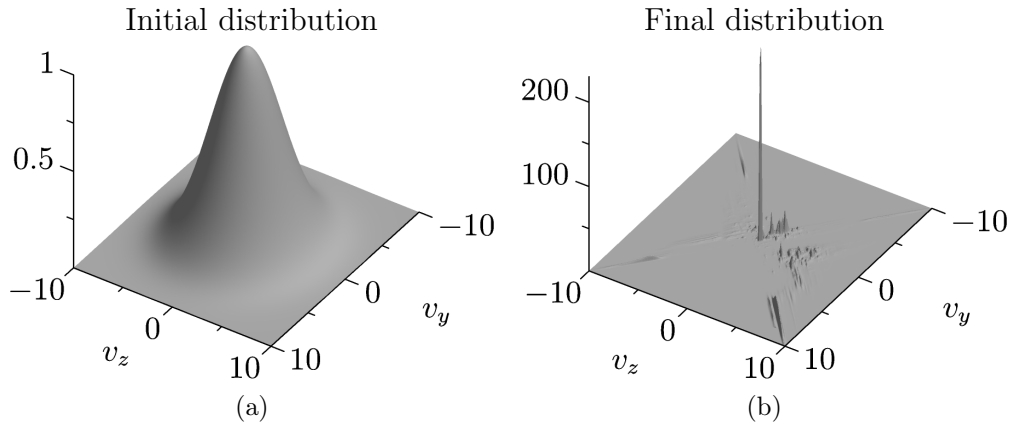

Figure 3.7: The velocity distribution of atoms when 2D Raman cooling by STIRAP starts (a) and ends (b). During the cooling, 500 elementary cycles have been applied, which results in the decrease of the velocity spread σ from (a) $3v_{\rm rec}$ to (b) $0.1v_{\rm rec}$ and the increase about 230 times of the central-peak height. The corresponding effective temperature goes down to $0.01T_{\rm rec}$. The scaling is given by the recoil velocity $v_{\rm rec} = \hbar k_P/M = \hbar k_S/M$.

Then equation (3.72) is written as

$$\sigma'_{11}(\mathbf{p}) = \sigma_{11}(\mathbf{p}) + \sigma_{33}^{++}(\mathbf{p} - \hbar\mathbf{k}_P + \Delta\mathbf{p}') + \sigma_{33}^{--}(\mathbf{p} - \hbar\mathbf{k}_P + \Delta\mathbf{p}''), \quad (3.74)$$

where the momentum shifts were changed in relation to $\mathcal{F}(\mathbf{p})$.

In contrast to the first step of cooling cycle, when atoms are held in the same momentum family $\mathcal{F}(\mathbf{p})$, Eq. (3.74) demonstrates that the second cooling step mixes different families $\mathcal{F}(\mathbf{p})$. Taking the average of Eq. (3.74) over all directions of spontaneous emission, one can see that the velocity distribution is generally pushed by a cooling cycle along the Oy axis. If the center $\mathbf{v}^0 = \mathbf{p}^0/M$ of the cross-like hole for atoms in state $|1\rangle$ (see Fig. 3.6c) is adjusted to $v_y^0 < 0$, then the cooling cycle pushes atoms with $v_y < 0$ closer to the zero velocity, stimulating a cooling of the atomic ensemble. In turn, an alternated laser configuration with a pump laser propagating in the opposite direction and adjustment to $v_y^0 > 0$ lead to a cooling of atoms with $v_y > 0$. As a result, whole the atomic ensemble is cooled by alternating these laser beam configurations.

During the cooling process, atoms are accumulated into a narrow peak centered at the zero velocity, which grows together with the number of cooling cycles. Figure 3.7 shows the result of 2D Raman cooling by STIRAP after 500 elementary cycles have been applied. One can see that the height

of the peak has increased about 230 times, starting from the initial broad distribution. Simultaneously, the spread $\sigma = (\mathrm{FWHM})/\sqrt{8\ln 2}$ of the velocity distribution has been reduced from $3v_{\mathrm{rec}}$ to $0.1v_{\mathrm{rec}}$. The effective temperature T_{eff} of the atomic ensemble goes down to $0.01T_{\mathrm{rec}}$, given in terms of the recoil-limit temperature T_{rec}.

2D Raman cooling by square pulses (paper IV) has the same behavior of the cooling process as shown above, but the difference in the mechanisms of population transfer leads to the following. Deep subrecoil cooling requires the very accurate and short duration of square pulses, whereas the duration of STIRAP does not influence on the velocity selectivity of the transfer but takes a much longer time. Hence, cooling by STIRAP is applicable if the cooling time is not in any critical role, providing the robustness against the pulse durations.

Chapter 4

Conclusions

This thesis investigates two different 2D methods, atom localization and Raman cooling, merged into one topic devoted to tripod-type atoms.

First, we have shown the high-precision 2D localization of a tripod-type atom after it passes an optical mask of light. Two perpendicular strong standing waves near-resonant to transitions of the atom induce a spatial inhomogeneity in atomic populations, with narrow localization domains within the optical wavelength λ. We select three spatial structures of the upper-state population such as spikes, craters and waves, which allow one to localize the atom within sub-wavelength domains of the width not limited by λ. The demonstrated method may find important practical applications in high-resolution atom lithography, which is of particular interest due to recent experiments with semiconductor elements [65–67].

Second, we have demonstrated efficient 2D Raman cooling of tripod-type atoms. Because such a cooling is sensitive to the form of coherent population transfer, we have considered for this purpose the transfer by square pulses and STIRAP. Both mechanisms lead to deep 2D cooling down to temperatures essentially below the one-photon recoil limit. On the other hand, the pulse durations needed by square pulses should be adjusted very accurately, but can be set in robust way for STIRAP. At the same time, the pulse duration of STIRAP is much longer than that of square pulse, hence, the use of STIRAP is preferable only if the cooling time is not in any critical role. The required theory of Raman cooling by STIRAP was first developed for 1D case and then extended to 2D. In addition, the momentum distribution of cold atoms has been derived for an arbitrary form of coherent population transfer, showing that cooling cycles can be reordered without the loss of cooling efficiency.

Our simplified treatment does not necessarily take into account many

aspects of an actual experiment, but it shows that *a priori* Raman cooling applied for tripod-type atoms may reach ultracold temperatures without the use of evaporative cooling. In addition to 3D cooling by thermalization, the approach can be used to cool atoms in an 1D optical lattice, where the sample is "sliced" into 2D pancake-like structures. This approach is used for investigating optical frequency standards with alkaline-earth atoms [28]. Also, for atomic clocks one needs high numbers of atoms and yet low densities to avoid interaction-induced frequency shifts, and one solution is again an optical lattice that slices the sample into non-interacting 2D pancakes [18]. Although then narrow-band cooling is the basic tool for e.g. alkaline earth atoms, one can also consider cooling at higher-lying atomic energy levels, which gives a rich level structure and opens the possibility for Raman cooling with tripod configuration.

Appendix A

Steady-state elements of density matrix

In this Appendix, we derive the steady-state solution for the density-matrix elements ρ_{ij} of Λ-type system shown in Fig. 2.3. The corresponding Eqs. (2.21) are written as

$$i\dot{\rho}_{11} = -g(\rho_{12} - \rho_{21}) + i\gamma_1\rho_{22}, \tag{A.1a}$$
$$i\dot{\rho}_{22} = g(\rho_{12} - \rho_{21}) - \Omega(\rho_{23} - \rho_{32}) - i\gamma\rho_{22}, \tag{A.1b}$$
$$i\dot{\rho}_{33} = \Omega(\rho_{23} - \rho_{32}) + i\gamma_2\rho_{22}, \tag{A.1c}$$
$$i\dot{\rho}_{12} = -g(\rho_{11} - \rho_{22}) - \Omega\rho_{13} + \Delta_1\rho_{12} - i\Gamma_{12}\rho_{12}, \tag{A.1d}$$
$$i\dot{\rho}_{13} = -\Omega\rho_{12} + g\rho_{23} - (\Delta_2 - \Delta_1)\rho_{13}, \tag{A.1e}$$
$$i\dot{\rho}_{23} = \Omega(\rho_{33} - \rho_{22}) + g\rho_{13} - \Delta_2\rho_{23} - i\Gamma_{23}\rho_{23}. \tag{A.1f}$$

Here, the dependence of the Rabi frequencies, g and Ω, on the position x of atom may have an arbitrary form. The steady state corresponds to relationships

$$\dot{\rho}_{ij} = 0, \quad i, j = 1, 2, 3. \tag{A.2}$$

Hence equation (A.1e) takes the form

$$\rho_{13} = \frac{-\Omega\rho_{12} + g\rho_{23}}{\delta}, \tag{A.3}$$

where $\delta = \Delta_2 - \Delta_1$ is the two-photon detuning between ground states $|1\rangle$ and $|3\rangle$. The substitution of Eq. (A.3) into Eqs. (A.1d) and (A.1f) produces

the following matrix equation for elements ρ_{12} and ρ_{23}:

$$\begin{pmatrix} \Gamma_{12} + i\Delta_1 + i\dfrac{\Omega^2}{\delta} & -i\dfrac{g\Omega}{\delta} \\ -i\dfrac{g\Omega}{\delta} & \Gamma_{23} - i\Delta_2 + i\dfrac{g^2}{\delta} \end{pmatrix} \begin{pmatrix} \rho_{12} \\ \rho_{23} \end{pmatrix} = \begin{pmatrix} igq_{12} \\ -i\Omega q_{32} \end{pmatrix}, \tag{A.4}$$

where $q_{m2} = \rho_{mm} - \rho_{22}$ $(m = 1, 3)$. It is straightforward to verify that the solution of this matrix equation is written as

$$\begin{pmatrix} \rho_{12} \\ \rho_{23} \end{pmatrix} = \frac{1}{\beta^*} \begin{pmatrix} \Gamma_{23} - i\Delta_2 + i\dfrac{g^2}{\delta} & i\dfrac{g\Omega}{\delta} \\ i\dfrac{g\Omega}{\delta} & \Gamma_{12} + i\Delta_1 + i\dfrac{\Omega^2}{\delta} \end{pmatrix} \begin{pmatrix} igq_{12} \\ -i\Omega q_{32} \end{pmatrix}, \tag{A.5}$$

where

$$\beta = \left(\Gamma_{12} - i\Delta_1 - i\frac{\Omega^2}{\delta}\right)\left(\Gamma_{23} + i\Delta_2 - i\frac{g^2}{\delta}\right) + \frac{g^2\Omega^2}{\delta^2}. \tag{A.6}$$

The imaginary parts of elements ρ_{12} and ρ_{23} are then given by

$$\operatorname{Im}\rho_{12} = q_{12}\frac{g}{|\beta|^2}\operatorname{Re}\left\{\beta\left(\Gamma_{23} - i\Delta_2 + i\frac{g^2}{\delta}\right)\right\} + q_{32}\frac{g\Omega^2}{\delta|\beta|^2}\operatorname{Im}\beta, \tag{A.7}$$

$$\operatorname{Im}\rho_{23} = -q_{12}\frac{g^2\Omega}{\delta|\beta|^2}\operatorname{Im}\beta - q_{32}\frac{\Omega}{|\beta|^2}\operatorname{Re}\left\{\beta\left(\Gamma_{12} + i\Delta_1 + i\frac{\Omega^2}{\delta}\right)\right\}. \tag{A.8}$$

Taking into account that

$$\rho_{22} = \frac{1 - q_{12} - q_{32}}{3}, \tag{A.9}$$

one can write Eqs. (A.1a) and (A.1c) in the form

$$\operatorname{Im}\rho_{12} = \frac{\gamma_1}{6g}(1 - q_{12} - q_{32}), \tag{A.10}$$

$$\operatorname{Im}\rho_{23} = -\frac{\gamma_2}{6\Omega}(1 - q_{12} - q_{32}). \tag{A.11}$$

Combining Eqs. (A.10) and (A.11) with Eqs. (A.7) and (A.8), one gets the matrix equation

$$MQ = \Gamma, \tag{A.12}$$

where the matrix M is written as

$$\begin{pmatrix} \frac{6g^2}{|\beta|^2}\,\mathrm{Re}\left\{\beta\left(\Gamma_{23}-i\Delta_2+i\frac{g^2}{\delta}\right)\right\}+\gamma_1 & \frac{6g^2\Omega^2}{\delta|\beta|^2}\,\mathrm{Im}\,\beta+\gamma_1 \\ \frac{6g^2\Omega^2}{\delta|\beta|^2}\,\mathrm{Im}\,\beta+\gamma_2 & \frac{6\Omega^2}{|\beta|^2}\,\mathrm{Re}\left\{\beta\left(\Gamma_{12}+i\Delta_1+i\frac{\Omega^2}{\delta}\right)\right\}+\gamma_2 \end{pmatrix}, \tag{A.13}$$

and the vectors in Eq. (A.12) are given by

$$Q=\begin{pmatrix} q_{12} \\ q_{32} \end{pmatrix}, \quad \Gamma=\begin{pmatrix} \gamma_1 \\ \gamma_2 \end{pmatrix}. \tag{A.14}$$

From the matrix equation (A.12), one derives variables q_{12} and q_{32}:

$$q_{12}=\frac{\gamma_1\Omega^2}{A}\,\mathrm{Re}(\beta\alpha_1), \tag{A.15}$$

$$q_{32}=\frac{\gamma_2 g^2}{A}\,\mathrm{Re}(\beta\alpha_2), \tag{A.16}$$

with the denominator

$$A=6\Gamma_{12}\Gamma_{23}g^2\Omega^2+\gamma_1\Omega^2\,\mathrm{Re}(\beta\alpha_1)+\gamma_2 g^2\,\mathrm{Re}(\beta\alpha_2), \tag{A.17}$$

the rest of values are given by

$$\alpha_1=\Gamma_{12}+i\Delta_1+i\frac{\zeta}{\gamma_1\delta}, \tag{A.18}$$

$$\alpha_2=\Gamma_{23}-i\Delta_2+i\frac{\zeta}{\gamma_2\delta}, \tag{A.19}$$

$$\zeta=\gamma_1\Omega^2+\gamma_2 g^2. \tag{A.20}$$

Finally, the populations of the Λ-type system are written as

$$\rho_{11}=\frac{\Omega^2}{A}\left(2\Gamma_{12}\Gamma_{23}g^2+\gamma_1\,\mathrm{Re}(\beta\alpha_1)\right), \tag{A.21}$$

$$\rho_{22}=\frac{2\Gamma_{12}\Gamma_{23}g^2\Omega^2}{A}, \tag{A.22}$$

$$\rho_{33}=\frac{g^2}{A}\left(2\Gamma_{12}\Gamma_{23}\Omega^2+\gamma_2\,\mathrm{Re}(\beta\alpha_2)\right). \tag{A.23}$$

Appendix B

Velocity selectivity of STIRAP

The case of large detuning Δ_P ($|\Delta_P| \gg \Omega_P(t), \Omega_S(t)$) allows us to consider an atom with arbitrary velocity v. For this purpose, we adiabatically eliminate the upper state $|2\rangle$, because it remains almost unpopulated during STIRAP. Hence, the probability function $|\Psi\rangle$ of atom satisfies approximation $\langle a_2|\frac{d}{dt}|\Psi\rangle \approx 0$, with the help of which contributions into state $|a_2\rangle$ are derived from the Hamiltonian (3.18):

$$\langle a_2|\Psi\rangle \approx \frac{\Omega_P(t)}{2\Delta_P}\langle a_1|\Psi\rangle + \frac{\Omega_S(t)}{2\Delta_P}\langle a_3|\Psi\rangle. \tag{B.1}$$

Here we use constraints $|\Delta_P| \gg \omega_R, kp/M$, and

$$|\langle a_2|\frac{d}{dt}|\Psi\rangle| \ll |\Delta_P||\langle a_2|\Psi\rangle|. \tag{B.2}$$

Equation (B.1) after the substitution into the left-hand side of Eq. (B.2) results in the following limitations:

$$|\Delta_S - \Delta_P|, T^{-1} \ll |\Delta_P|. \tag{B.3}$$

Taking into account Eq. (B.1), the Hamiltonian (3.18) is reduced to the Hamiltonian of effective two-level system

$$\hat{H}_{\text{eff}} = \frac{\hbar}{2}\begin{pmatrix} -2\delta_0(t) & \Omega_{\text{eff}}(t) \\ \Omega_{\text{eff}}(t) & 2(\delta_{\text{eff}}(t) - \delta_0(t)) \end{pmatrix}, \tag{B.4}$$

with the effective Rabi frequency and detunings

$$\Omega_{\text{eff}}(t) = \frac{\Omega_P(t)\Omega_S(t)}{2\Delta_P}, \tag{B.5a}$$

$$\delta_0(t) = -\frac{\Omega_P^2(t)}{4\Delta_P}, \tag{B.5b}$$

$$\delta_{\text{eff}}(t) = \Delta\delta + \frac{\Omega_S^2(t) - \Omega_P^2(t)}{4\Delta_P}, \tag{B.5c}$$

where $\Delta\delta = \Delta_S - \Delta_P + 2kp/M = 2k(v - v_0)$.

B.1 The eigenstates of the effective Hamiltonian

The eigenstates of the effective Hamiltonian (B.4) are given by

$$|a_+\rangle = \sin\Theta|a_1\rangle + \cos\Theta|a_3\rangle, \tag{B.6a}$$

$$|a_-\rangle = \cos\Theta|a_1\rangle - \sin\Theta|a_3\rangle, \tag{B.6b}$$

where the mixing angle Θ is

$$\tan\Theta = \sqrt{1 + \frac{\delta_{\text{eff}}^2}{\Omega_{\text{eff}}^2}} - \frac{\delta_{\text{eff}}}{\Omega_{\text{eff}}}. \tag{B.7}$$

The corresponding eigenfrequencies are

$$\omega_\pm = -\delta_0 + \frac{\delta_{\text{eff}}}{2} \pm \frac{\Omega_{\text{eff}}}{2}\sqrt{1 + \delta_{\text{eff}}^2/\Omega_{\text{eff}}^2}. \tag{B.8}$$

In terms of eigenstates $|a_+\rangle$ and $|a_-\rangle$, the two-photon resonance (3.34) corresponds to $\Delta\delta = 0$. In this case, Eq. (B.7) for the mixing angle Θ is reduced to Eq. (3.38), and eigenstates $|a_+\rangle$, $|a_-\rangle$ coincide with states $|\text{C}\rangle$ and $|\text{NC}\rangle$, respectively. The adiabatic population transfer from the $|a_1\rangle$ to the $|a_3\rangle$ state is accomplished by the non-coupled eigenstate $|\text{NC}\rangle$ during the period when the angle Θ changes from 0 to $\pi/2$. Hence, the eigenvalue ω_{NC} starts from the frequency of $|a_1\rangle$ and ends at the frequency of $|a_3\rangle$. One can apply this qualitative picture for the case of $\delta \neq 0$, replacing the non-coupled state $|\text{NC}\rangle$ by state $|a_-\rangle$. To ensure that population transfer by STIRAP occurs, we follow eigenvalues $\omega_\pm$, the dependence of which on detuning δ_{eff} is shown in Fig. B.1. During the overlapping period $\Delta\tau$, the

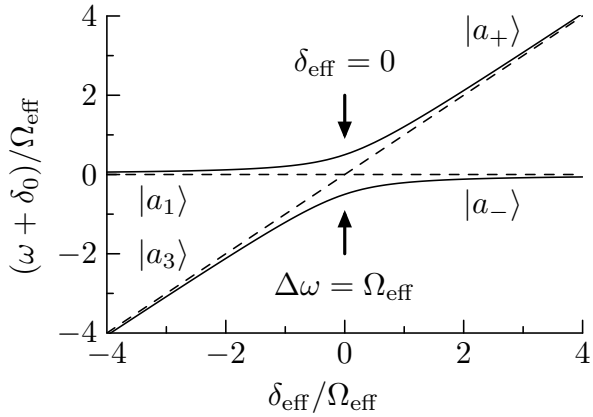

Figure B.1: The eigenfrequencies of bare atomic states $|a_1\rangle$ and $|a_3\rangle$ (dashed lines) cross at point $\delta_{\text{eff}}=0$. The level crossing avoided for the eigenstates (solid lines) changes the association between eigenstates and bare atomic states.

sign of δ_{eff} changes from positive to negative or vice versa, depending on the sign of Δ_P. The zero value of δ_{eff} determines the point where the switching between states $|a_1\rangle$ and $|a_3\rangle$ appears.

Figure B.2 shows the eigenfrequencies $\omega_\pm$ as functions of time, where the behavior of the detuning δ_{eff} defines three possible cases: (a) $\delta_{\text{eff}}>0$ or (b) $\delta_{\text{eff}}<0$ during the overlapping period $\Delta\tau$ of laser pulses; (c) $\delta_{\text{eff}}=0$ at some moment of this period. Adiabatic transfer is suppressed in Figs. B.2a and B.2b, because both eigenstates $|a_+\rangle$ and $|a_-\rangle$ come back to the initial bare state as the STIRAP ends. Adiabatic transfer is only accomplished in Fig. B.2c, where the crossing between the frequencies of bare states $|a_1\rangle$ and $|a_3\rangle$ occurs, and dressed state $|a_-\rangle$ carries out population from state $|a_1\rangle$ to $|a_3\rangle$. The explicit expression (B.5c) of δ_{eff} gives the velocity range of the adiabatic transfer in the form

$$-\frac{\Omega_{S0}^2}{8k|\Delta_P|}<v-v_0<\frac{\Omega_{P0}^2}{8k|\Delta_P|}\quad\text{if }\Delta_P>0, \tag{B.9a}$$

$$-\frac{\Omega_{P0}^2}{8k|\Delta_P|}<v-v_0<\frac{\Omega_{S0}^2}{8k|\Delta_P|}\quad\text{if }\Delta_P<0. \tag{B.9b}$$

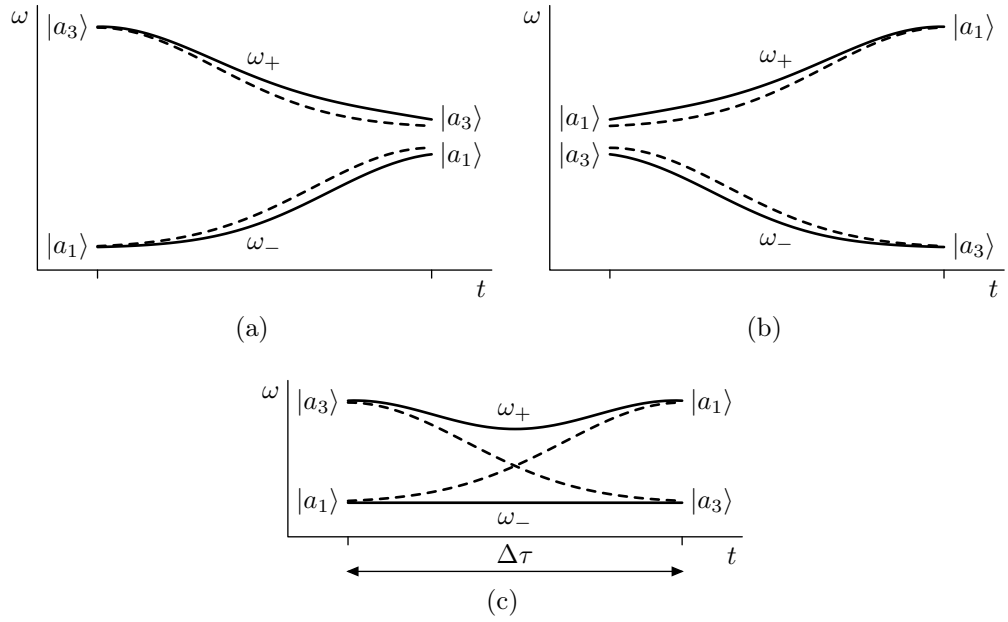

Figure B.2: The time dependence of the dressed-state eigenfrequencies (solid line) over the overlapping period $\Delta\tau$ of laser pulses. The frequencies of the bare atomic states are shown in dashed lines. There are three possible cases in dependence on $\Delta\delta$: (a) $\delta_{\text{eff}} > 0$, (b) $\delta_{\text{eff}} < 0$ over all this period; (c) $\delta_{\text{eff}} = 0$ at a specific time. (c) corresponds to adiabatic transfer from the $|a_1\rangle$ to $|a_3\rangle$ state.

B.2 Resonant velocity group

For adiabatic transfer, detunings $\delta_{\text{eff}}(t)$ and $\delta_0(t)$, and Rabi frequency $\Omega_{\text{eff}}(t)$ should evolve in time very slowly to neglect the mixing between dressed states $|a_+\rangle$ and $|a_-\rangle$. Then a transferred atom remains in the $|a_-\rangle$ state until the STIRAP ends, and the atom comes to state $|a_3\rangle$ from $|a_1\rangle$. If such a condition is satisfied for all atomic velocities, then Eq. (B.9) corresponds to the velocity range of population transfer. As a result, the probability of the transfer within the range (B.9) is near unity, whereas the rest of atoms are not affected. However, the adiabaticity criterion for huge velocities can not be sustained, because it requires too long pulse durations, suppressing effective cooling. In contrast, our suggestion is to adiabatically transfer only atoms at the resonant velocity (3.34), which requires a much shorter duration of STIRAP.

In the case of large detuning Δ_P, the adiabaticity criterion reads

$$|\langle a_+|\frac{d}{dt}|a_-\rangle| \ll |\omega_+ - \omega_-|. \tag{B.10}$$

We transform this constraint, substituting dressed states $|a_+\rangle$, $|a_-\rangle$ from Eq. (B.6) and frequencies $\omega_\pm$ from Eq. (B.8) to the form

$$|\dot{\Theta}| \ll \sqrt{\Omega_{\text{eff}}^2 + \delta_{\text{eff}}^2}. \tag{B.11}$$

Similarly to Eq. (3.41), Eq. (B.11) leads to the "global" adiabaticity criterion after the replacement of derivative $\dot{\Theta}$ by its average value $\langle\dot{\Theta}_{av}\rangle$.

Whether population transfer between states $|a_1\rangle$ and $|a_3\rangle$ is adiabatic or not, the largest rate of the transfer corresponds to the two-photon resonance. On the other hand, for atoms adiabatically following dressed state $|a_-\rangle$, population in bare state $|a_3\rangle$ changes as $\sin^2\Theta$, so that it has a similar behavior to the mixing angle Θ. Thus we can assume that the largest rate of Θ corresponds to the two-photon resonance as well, at least for large enough $\Delta\tau$. As a result, the average value $\langle\dot{\Theta}_{av}\rangle$ satisfies the inequality

$$\langle\dot{\Theta}_{av}\rangle \leq \frac{\pi}{2}\Delta\tau. \tag{B.12}$$

Figures B.2a and B.2b demonstrate cases where for each atomic state population is the same at the beginning and at the end of STIRAP, however the mixing angle Θ may take significant values from 0 to $\pi/4$. Hence the order of magnitude of $\langle\dot{\Theta}_{av}\rangle$ is about $\Delta\tau^{-1}$. Explicit forms (B.5) of $\Omega_{\text{eff}}(t)$, $\delta_{\text{eff}}(t)$ allows us to rewrite Eq. (B.11) as

$$\frac{1}{\Delta\tau} \ll \sqrt{\left(\frac{\Omega_P^2(t) + \Omega_S^2(t)}{4\Delta_P}\right)^2 + \Delta\delta\left(\Delta\delta + \frac{\Omega_S^2(t) - \Omega_P^2(t)}{2\Delta_P}\right)}. \tag{B.13}$$

Equation (B.13) is reduced to the adiabaticity criterion (3.42) in the case of the two-photon resonance due to $\Delta\delta = 0$. Hence adiabatic transfer of population takes place for the resonant atoms and those of them, for which the following condition is valid:

$$\Delta\delta\left(\Delta\delta + \frac{\Omega_S^2(t) - \Omega_P^2(t)}{2\Delta_P}\right) \geq 0. \tag{B.14}$$

In accordance with this inequality, velocity groups of the adiabatic transfer are given by

$$v - v_0 \leq -\frac{\Omega_{S0}^2}{4k|\Delta_P|} \quad \text{or} \quad v - v_0 \geq \frac{\Omega_{P0}^2}{4k|\Delta_P|} \quad \text{if } \Delta_P > 0, \tag{B.15a}$$

$$v - v_0 \leq -\frac{\Omega_{P0}^2}{4k|\Delta_P|} \quad \text{or} \quad v - v_0 \geq \frac{\Omega_{S0}^2}{4k|\Delta_P|} \quad \text{if } \Delta_P < 0. \tag{B.15b}$$

One can see that, in these cases, Θ equals 0 when STIRAP ends, causing atoms to come back to state $|a_1\rangle$. As these atoms are not transferred, only the atoms in velocity range

$$-\frac{\Omega_{S0}^2}{4k|\Delta_P|} < v - v_0 < \frac{\Omega_{P0}^2}{4k|\Delta_P|} \quad \text{if } \Delta_P > 0, \tag{B.16a}$$

$$-\frac{\Omega_{P0}^2}{4k|\Delta_P|} < v - v_0 < \frac{\Omega_{S0}^2}{4k|\Delta_P|} \quad \text{if } \Delta_P < 0, \tag{B.16b}$$

can reach state $|a_3\rangle$.

Bibliography

[1] C. Pethick and H. Smith, *Bose-Einstein Condensation in Dilute Gases* (Cambridge University Press, 2008).

[2] T. Grunzweig, A. Hilliard, M. McGovern, and M. F. Andersen, Nature **6**, 951 (2010).

[3] R. J. Schoelkopf and S. M. Girvin, Nature **451**, 664 (2008).

[4] J. Clarke and F. K. Wilhelm, Nature **453**, 1031 (2008).

[5] L. Sander, *Advanced Condensed Matter Physics* (Cambridge University Press, 2009).

[6] J. Weiner, V. S. Bagnato, S. Zilio, and P. S. Julienne, Rev. Mod. Phys. **71**, 1 (1999).

[7] M. Roghani and H. Helm, Phys. Rev. A **77**, 043418 (2008).

[8] M. Roghani, H. Helm, and H.-P. Breuer, Phys. Rev. Lett. **106**, 040502 (2011).

[9] M. Roghani, H.-P. Breuer, and H. Helm, Phys. Rev. A **85**, 012313 (2012).

[10] S. E. Harris, Physics Today **50**, 36 (1997).

[11] G. Alzetta, A. Gozzini, L. Moi, and G. Orriols, Nuovo Cimento B **36**, 5 (1976).

[12] H. R. Gray, R. M. Whitley, and J. C. R. Stroud, Opt. Lett. **3**, 218 (1978).

[13] R. Abfalterer, C. Keller, S. Bernet, M. K. Oberthaler, J. Schmiedmayer, and A. Zeilinger, Phys. Rev. A **56**, R4365 (1997).

[14] C. Keller, R. Abfalterer, S. Bernet, M. K. Oberthaler, J. Schmiedmayer, and A. Zeilinger, Vac. Sci. Technol. B **16**, 3850 (1998).

[15] K. S. Johnson, J. H. Thywissen, N. H. Dekker, K. K. Berggren, A. P. Chu, R. Younkin, and M. Prentiss, Science **280**, 1583 (1998).

[16] C. Audoin and B. Guinot, *The Measurement of Time: Time, Frequency and the Atomic Clock* (Cambridge University Press, 2001).

[17] J. Ye, H. J. Kimble, and H. Katori, Science **320**, 1734 (2008).

[18] A. Derevianko and H. Katori, Rev. Mod. Phys. **83**, 331 (2011).

[19] M. Nielsen and I. Chuang, *Quantum Computation and Quantum Information* (Cambridge University Press, 2000).

[20] S. Stenholm and K.-A. Suominen, *Quantum Approach to Informatics* (Wiley, 2005).

[21] G. S. Agarwal and K. T. Kapale, J. Phys. B: At. Mol. Opt. Phys. **39**, 3437 (2006).

[22] H. Metcalf and P. Van der Straten, *Laser cooling and trapping* (Springer-Verlag GmbH, 1999).

[23] M. Weidemüller and C. Zimmermann, *Cold Atoms and Molecules* (Wiley, 2009).

[24] C. Cohen-Tannoudji and D. Guéry-Odelin, *Advances In Atomic Physics: An Overview* (World Scientific Publishing Company, Incorporated, 2011).

[25] W. Ketterle and N. J. V. Druten, Adv. At. Mol. Opt. Phys. **37**, 181 (1996).

[26] M. Haas, V. Leung, D. Frese, D. Haubrich, S. John, C. Weber, A. Rauschenbeutel, and D. Meschede, New J. Phys **9**, 147 (2007).

[27] R. Wynands and S. Weyers, Metrologia **42**, S64 (2005).

[28] M. M. Boyd, A. D. Ludlow, S. Blatt, S. M. Foreman, T. Ido, T. Zelevinsky, and J. Ye, Phys. Rev. Lett. **98**, 083002 (2007).

[29] C. N. Cohen-Tannoudji and W. D. Phillips, Physics Today **43**, 33 (1990).

[30] J. Dalibard and C. Cohen-Tannoudji, J. Opt. Soc. Am. B **2**, 1707 (1985).

[31] J. Dalibard and C. Cohen-Tannoudji, J. Opt. Soc. Am. B **6**, 2023 (1989).

[32] A. Aspect, E. Arimondo, R. Kaiser, N. Vansteenkiste, and C. Cohen-Tannoudji, Phys. Rev. Lett. **61**, 826 (1988).

[33] M. Kasevich and S. Chu, Phys. Rev. Lett. **69**, 1741 (1992).

[34] A. M. Herkommer, W. P. Schleich, and M. S. Zubairy, J. Mod. Opt. **44**, 2507 (1997).

[35] S. Qamar, S.-Y. Zhu, and M. Zubairy, Opt. Commun. **176**, 409 (2000).

[36] S. Qamar, S.-Y. Zhu, and M. S. Zubairy, Phys. Rev. A **61**, 063806 (2000).

[37] E. Paspalakis and P. L. Knight, Phys. Rev. A **63**, 065802 (2001).

[38] E. Paspalakis, A. F. Terzis, and P. L. Knight, J. Mod. Opt. **52**, 1685 (2005).

[39] W. Heisenberg, Zeitschrift für Physik **43**, 172 (1927).

[40] N. Davidson, H. J. Lee, M. Kasevich, and S. Chu, Phys. Rev. Lett. **72**, 3158 (1994).

[41] V. Boyer, L. J. Lising, S. L. Rolston, and W. D. Phillips, Phys. Rev. A **70**, 043405 (2004).

[42] E. S. Shuman, J. F. Barry, and D. Demille, Nature **467**, 820 (2010).

[43] V. Gokhroo, G. Rajalakshmi, R. K. Easwaran, and C. S. Unnikrishnan, J. Phys. B: At. Mol. Opt. Phys. **44**, 115307 (2011).

[44] M. Landini, S. Roy, L. Carcagní, D. Trypogeorgos, M. Fattori, M. Inguscio, and G. Modugno, Phys. Rev. A **84**, 043432 (2011).

[45] P. Phoonthong, P. Douglas, A. Wickenbrock, and F. Renzoni, Phys. Rev. A **82**, 013406 (2010).

[46] M. A. Ol'shanii and V. G. Minogin, Quantum Opt. **3**, 317 (1991).

[47] H. Theuer, R. Unanyan, C. Habscheid, K. Klein, and K. Bergmann, Opt. Express **4**, 77 (1999).

[48] F. Vewinger, M. Heinz, R. Garcia Fernandez, N. V. Vitanov, and K. Bergmann, Phys. Rev. Lett. **91**, 213001 (2003).

[49] J. E. Thomas, Phys. Rev. A **42**, 5652 (1990).

[50] K. D. Stokes, C. Schnurr, J. R. Gardner, M. Marable, G. R. Welch, and J. E. Thomas, Phys. Rev. Lett. **67**, 1997 (1991).

[51] J. R. Gardner, M. L. Marable, G. R. Welch, and J. E. Thomas, Phys. Rev. Lett. **70**, 3404 (1993).

[52] P. Storey, M. Collett, and D. Walls, Phys. Rev. Lett. **68**, 472 (1992).

[53] P. Storey, M. Collett, and D. Walls, Phys. Rev. A **47**, 405 (1993).

[54] P. Storey, T. Sleator, M. Collett, and D. Walls, Phys. Rev. A **49**, 2322 (1994).

[55] S. Kunze, G. Rempe, and M. Wilkens, Europhys. Lett. **27**, 115 (1994).

[56] S. H. Autler and C. H. Townes, Phys. Rev. **100**, 703 (1955).

[57] P. Knight and P. Milonni, Physics Reports **66**, 21 (1980).

[58] K. Blum, *Density Matrix Theory and Applications* (Springer, 2010).

[59] J. Reichel, F. Bardou, M. B. Dahan, E. Peik, S. Rand, C. Salomon, and C. Cohen-Tannoudji, Phys. Rev. Lett. **75**, 4575 (1995).

[60] F. Bardou, J. P. Bouchaud, O. Emile, A. Aspect, and C. Cohen-Tannoudji, Phys. Rev. Lett. **72**, 203 (1994).

[61] J. Reichel, O. Morice, G. M. Tino, and C. Salomon, Europhys. Lett. **28**, 477 (1994).

[62] M. P. Fewell, B. W. Shore, and K. Bergmann, Aust. J. Phys. **50**, 281 (1997).

[63] K. Bergmann, H. Theuer, and B. W. Shore, Rev. Mod. Phys. **70**, 1003 (1998).

[64] A. Messiah, *Quantum Mechanics: Two Volumes Bound As One* (Dover Publications, Incorporated, 1999).

[65] S. J. Rehse, K. M. Bockel, and S. A. Lee, Phys. Rev. A **69**, 063404 (2004).

[66] R. Chen, J. F. McCann, and I. Lane, J. Phys. B: At. Mol. Opt. Phys. **40**, 1535 (2007).

[67] B. Klöter, C. Weber, D. Haubrich, D. Meschede, and H. Metcalf, Phys. Rev. A **77**, 033402 (2008).